SPARK PLASMA SINTERING OF MAGNESIUM MATRIX COMPOSITES

By

ANIRUDDHA DAS

Bachelor of Science in Mechanical Engineering

Bangladesh University of Engineering and Technology

Dhaka, Bangladesh

2009

Submitted to the Faculty of the
Graduate College of the
Oklahoma State University
in partial fulfillment of
the requirements for
the Degree of
MASTER OF SCIENCE
December, 2012

SPARK PLASMA SINTERING OF MAGNESIUM

MATRIX COMPOSITES

Thesis Approved:

Dr. Sandip P. Harimkar

Thesis Adviser

Dr. Hamed Hatami-Marbini

Dr. Raman P. Singh

Dr. Sheryl A. Tucker

Dean of the Graduate College

TABLE OF CONTENTS

Chapter Page

I. INTRODUCTION 1

1.1 Introduction…….. 1

1.2 Reinforcements in Mg matrix…….. 2

1.2.1 Particle……. 2

1.2.2 Whisker or short fiber……. 3

1.2.3 Continuous fiber…….. 3

1.3 Challenges in making Mg matrix composites…….. 4

1.4 Processing of Mg matrix composites……... 4

1.4.1 Casting……. 5

1.4.1.1 Die casting……... 6

1.4.1.2 Semi-solid casting……... 6

1.4.1.3 Squeeze casting……... 7

1.4.1.4 Stir casting……... 8

1.4.2 Spray processing……. 9

1.4.3 Disintegrated melt deposition technique……. 10

1.4.4 Powder metallurgy…….. 11

1.4.4.1 Hot pressing……. 12

1.4.4.2 Hot isostatic pressing…….. 13

1.4.4.3 Spark plasma sintering…… 13

1.5 Role of spark plasma sintering process parameters…… 13

1.5.1 Effect of heating rate…… 15

1.5.2 Effect of pressure……. 17

1.5.3 Effect of electric current…….. 19

1.6 Mg based composites: a review……..... 20

1.6.1 Ceramic particle reinforced Mg matrix composites……. 20

1.6.1.1 Al_2O_3 reinforcement……. 21

1.6.1.2 TiC reinforcement…… 23

1.6.1.3 SiC reinforcement…… 23

1.6.2 Carbon allotropes reinforced Mg matrix composites……... 24

1.6.2.1 Carbon nanotubes…… 25

1.6.2.2 Graphene……..... 27

1.7 Objectives……. 28

II. EXPERIMENTAL DETAILS **29**

2.1 Materials……... 29

2.2 Processing of the composites……... 30

2.2.1 Milling process……. 30

2.2.2 Spark plasma sintering……. 31

2.3 Characterization of the composites……... 33

2.3.1 Density measurement…….. 34

2.3.2 Phase analysis…….. 35

2.3.3 Microhardness testing…….. 35

2.3.4 Compression testing……. 35

2.3.5 Wear testing……. 35

III. RESULTS AND DISCUSSION 37

3.1 Spark plasma sintering of GPL reinforced Mg matrix composites……... 37

3.1.1 Density……. 37

3.1.2 X-ray diffraction analysis……..... 38

3.1.3 Mechanical properties characterization……... 39

3.1.3.1 Microhardness testing…….. 39

3.1.3.2 Compression testing……. 41

3.1.3.3 Fracture behavior……. 42

3.1.4 Tribological behavior……... 44

3.2 Spark plasma sintering of nano-SiC reinforced Mg matrix composites…... 51

3.2.1 Density……. 51

3.2.2 X-ray diffraction analysis…… 51

3.2.3 Mechanical properties characterization……... 52

3.2.3.1 Microhardness testing…….. 52

3.2.3.2 Compression testing…… 53

3.2.3.3 Fracture behavior……. 55

3.2.4 Tribological behavior…….. 57

IV. CONCLUSIONS **62**

V. FUTURE WORKS **64**

REFERENCES **65**

LIST OF TABLES

Table Page

2.1 Specifications of the materials used in this study…… 29

3.1 Density of Mg-GPL composites…… 38

3.2 Density of Mg-nano SiC composites…… 51

LIST OF FIGURES

Figure		Page
Fig. 1.1	Classification of processing methods of Mg matrix composites……..	5
Fig. 1.2	Squeeze casting technique to fabricate Mg matrix composites [23]…..	7
Fig. 1.3	Schematic diagram showing stir casting process [25]……	9
Fig. 1.4	Schematic diagram of disintegrated melt deposition method [36] (Reprinted with permission from Elsevier)……	11
Fig. 1.5	Schematic showing spark plasma sintering mechanism [51] (Reprinted with permission from Elsevier)……	15
Fig. 1.6	Effect of pressure on the temperature required to achieve 95% density and grain size for ZrO_2 [45] (Reprinted with permission from Elsevier)……	18
Fig. 1.7	Effect of applied pressure on relative density and grain size of cubic ZrO_2 [45] (Reprinted with permission from Elsevier)……..	19
Fig. 1.8	Optical micrographs of (a) pure Mg, and (b) Mg-Al_2O_3 wrought materials [69] (Reprinted with permission from Elsevier)……...	22

Fig. 1.9 SEM images of (a) pure Mg powders, and (b-d) Mg powders coated with CNTs after drying at 80° C in atmosphere. Arrows indicate some surfactants in the form of solid [81] (Reprinted with permission from Elsevier)……..... 27

Fig. 2.1 High energy ball milling machine…… 30

Fig. 2.2 Glove box used for handling of Mg materials…….. 31

Fig. 2.3 Spark plasma sintering machine and its important components……... 33

Fig. 2.4 Nanovea Tribometer……. 36

Fig. 2.5 Nanovea optical 3-D Profilometer…… 36

Fig. 3.1 X-ray diffraction patterns from SPS sintered Mg and Mg-GPL composites…… 39

Fig. 3.2 Microhardness data of Mg-GPL composites…… 40

Fig. 3.3 Stress-strain diagram of pure Mg, Mg-1% GPL, Mg-2% GPL, and Mg-5% GPL …… 41

Fig. 3.4 Macrographs of pure Mg, Mg-2% GPL, and Mg-5% GPL samples after compressive fracture……. 42

Fig. 3.5 Fractured surfaces of (a) pure Mg, and (b) Mg-2% GPL showing formation of shear bands……... 43

Fig. 3.6 SEM images of fractured surfaces of (a) pure Mg, (b) Mg-2% GPL, (c) Mg-5% GPL, and (d) high magnification image of Mg-5 % GPL……... 44

Fig. 3.7 Wear loss as a function of sliding time for pure Mg and Mg-GPL composites……..... 45

Fig. 3.8 Friction coefficient as a function of sliding time for (a) pure Mg, (b) Mg-5% GPL, and (c) average friction coefficient as a function of sliding time for pure Mg, Mg-1% GPL, Mg-2% GPL, Mg-5% GPL….. 47

Fig. 3.9 Surface profiles for wear tracks of (a) pure Mg, (b) Mg-5% GPL, and (c) depth profiles across the wear tracks of pure Mg and Mg-5% GPL composites……..... 48

Fig. 3.10 Wear tracks of SPS sintered (a) pure Mg, (b) Mg-2% GPL, (c) Mg-5 % GPL, and (d) high magnification image of Mg-5% GPL showing broken graphene platelets on wear track……... 50

Fig. 3.11 X-ray diffraction patterns from SPS sintered Mg and Mg-nano SiC composites……..... 52

Fig. 3.12 Microhardness data of Mg-nano SiC composites……... 53

Fig. 3.13 Compression testing data of Mg-nano SiC composites…… 55

Fig. 3.14 Macrographs of Mg, Mg-2% nano SiC, and Mg-4% nano SiC samples after compressive fracture……. 55

Fig. 3.15 Fractured surfaces of (a) Mg-2% nano SiC, (b) Mg-4% nano SiC showing shear bands, (c) high magnification SEM images of Mg-2% nano SiC, and (d) Mg-4% nano SiC ……... 56

Fig. 3.16 Cumulative weight loss as a function of sliding time for different Mg-nano SiC composites……. 58

Fig. 3.17 Friction coefficient as a function of sliding time for (a) pure Mg, (b) Mg-2% nano SiC, and (c) average friction coefficient as a function of sliding time for Mg-nano SiC composites having different SiC contents…… 59

Fig. 3.18 Surface profiles for wear tracks of (a) pure Mg, (b) Mg-2% nano SiC, and (c) depth profiles across the wear tracks of Mg and Mg-nano SiC... 60

Fig. 3.19 Wear tracks of SPS sintered (a) pure Mg, (b) Mg-2% nano SiC, (c) Mg-4% nano SiC, and (d) high magnification image of Mg-4% nano SiC showing agglomerated SiC particles on wear track…….... 61

CHAPTER I

INTRODUCTION

1.1 Introduction

Magnesium (Mg) is the eighth most abundant element on earth, consisting approximately 2.7% by weight of the Earth's crust [1]. Mg exhibits low density (~1.74 g/cm^3) and excellent formability. Mg is the lightest among all structural materials; its density is approximately two-third of the density of aluminum and one-fifth of steel. It has better ductility, noise and vibration dampening properties compared to aluminum [2]. It can be easily machined, cast, forged, and welded. However, low strength and poor wear resistance limits the application of Mg in structural applications [3- 5].

Magnesium can be alloyed with Al, Mn, Zn, Zr and rare earth elements [6]. Alloying improves some of the properties, particularly strength, corrosion resistance and heat resistance, and makes it an important material for structural applications. Some of the well-known Mg alloys are AZ91 (9% Al-0.7% Zn-0.13% Mn; good room temperature strength and castability), AZ31 (3% Al-1% Zn-0.2% Mn; good weldability), AM60 (6% Al-0.15% Mn; good toughness and ductility), ZK60 (5–6% Zn-0.3–0.9% Zr; good room temperature strength and ductility), ZE41 (4.2% Zn-0.7% Zr-1.2% rare earth element; good creep strength and heat resistance), WE54 (Mg-5.1%Y-3.25%Nd-0.5% Zr; good creep strength and corrosion resistance) and AS41 (4.2%Al-1%Si; good creep strength up to 150°C). Mg alloys are used in aerospace and automobile

industries as a replacement of steel and aluminum. They are also used as a replacement of plastics in electronics and computer industries. Mg alloys have been used or considered for use in automobiles for various parts such as steering columns, engine blocks and transmission cases, gear box and clutch housing, instrument panels, wheels, and seat frames. These alloys have also been used to make gearbox housing, airframes and landing wheels of aircrafts because of their excellent vibration damping properties. Some of the recent applications of Mg alloys are for the cases of laptops, cell phones and cameras because of their light weight, heat and moisture resistance characteristics, and ability to minimize noise and vibration.

While the alloying elements can improve the strength, other properties such as low coefficient of thermal expansion, high elastic modulus and good wear resistance can only be improved by adding a strong and stiff second phase material [7, 8]. To improve the properties of Mg, different types of reinforcements have been incorporated with Mg materials.

1.2 Reinforcements for Mg matrix

Proper selection of reinforcement is an important factor to improve the properties of the matrix material. The selection of reinforcement is done based on the size and shape of the particles, processing method, manufacturing cost and desired properties of the composite [9, 10]. If the composite is to be used in structural application, then the density, modulus and strength are the primary considerable factors. Uniform distribution of reinforcements is also another important factor to improve the properties.

1.2.1 Particle

Particle reinforced Mg matrix composites can be processed using similar fabrication technique of monolithic Mg due to the homogeneous properties of the particles. That's why the processing cost was also lower compared to other reinforcements. Two basic types of manufacturing

methods are used to reinforce particles in Mg matrix: powder metallurgy and molten metal methods. In powder metallurgy, the particles are mixed with the Mg powders to achieve a homogeneous mixture. To achieve this, the size of the reinforcement and the size of the matrix particles are the influencing factors. In molten state processes, the reaction between particle and matrix, and reinforcement particle size are influencing factors. For example, Al_2O_3 is unstable in molten Mg alloys and forms Al_2MgO_4 [10]. Coarse particles are easier to incorporate into the Mg melt, but the fine particles increase the viscosity of the melt, and make the process difficult.

1.2.2 Whisker or short fiber

Whiskers or short fibers are commercially available in the form of preforms. The greater load bearing and transferring capabilities of short fibers give better mechanical properties compared to particle reinforcements. In some applications, the anisotropic property of a material is an important factor which cannot be achieved using particle reinforcements but can be achieved incorporating short fibers or whiskers. Among all discontinuously reinforced Mg-matrix composites, SiC whisker reinforced Mg-matrix composites show better properties due to the intrinsic properties of SiC whiskers [11]. But the application of SiC whisker reinforced Mg-matrix composite is limited due to the high cost of SiC whisker.

1.2.3 Continuous fiber

In continuous fiber reinforced composites, elongated fibers (aspect ratio $\geq$ 10) are used. These composites give very high strength and stiffness along the fiber direction, and these properties can be controlled macroscopically. Young's modulus can be drastically increased using high modulus fibers. The most common continuous fiber reinforcements in Mg-matrix are graphite and alumina fibers.

1.3 Challenges in making Mg matrix composites

The most critical issues in the fabrication of Mg matrix composites are 1) the dispersion of reinforcements in the magnesium matrix, 2) interfacial bond between the matrix and the reinforcements, and 3) controlling of unknown interfacial reaction between the matrix and the reinforcements. Proper dispersion of reinforcement is the main challenge to make Mg composites. If dispersion is not good, reinforcing materials will form clusters due to agglomeration. If the interfacial bond is weak then the effectiveness of reinforcement will not work. This reinforcement will act as a source of inclusions and the failure will occur at matrix-reinforcement interfaces. In some cases, undesired chemical reaction between reinforcements and matrix severely degrade the properties of the composites.

1.4 Processing of Mg matrix composites

Mg matrix composites can be processed using both liquid state processing and solid state processing methods. Liquid state processing methods, which are also known as molten metal methods, include casting, spray processing, disintegrated melt deposition technique (DMD) etc. Solid state processing methods are usually called powder metallurgy techniques. Fig. 1.1 shows classifications of various processing methods of Mg matrix composites.

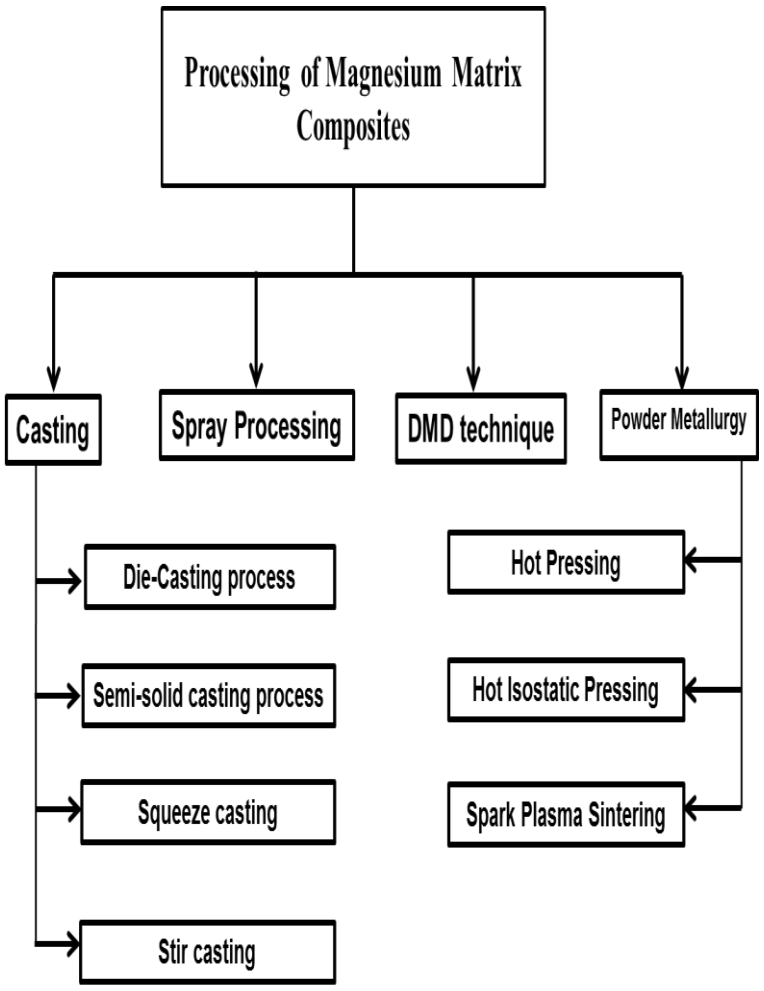

Fig. 1.1 Classification of processing methods of Mg matrix composites

1.4.1 Casting

Casting is the most economical process among all processing routes for Mg matrix composites. In a casting method, the molten metal is directly poured into the mold having desired shape and size. However, casting methods have some drawbacks such as formation of casting defects, including blow holes, porosity, etc. [12]. Minimizations of these defects can be done by modifying the casting process. These modified casting processes are known as die-casting, squeeze casting, stir casting, etc.

1.4.1.1 Die casting

Die casting is a material processing method where molten metal is poured into the mold cavity using high pressure. Die casting allows good castability of Mg matrix composites. Mg has better flow properties compared to aluminum and zinc, allowing molding of thin-walled parts. Thin structural parts of automotive industries can easily be made using casting methods [13].

Mg-die casting is also favorable compared to aluminum and zinc die-casting because of its low casting temperature and low thermal energy needed. Low casting temperature and low thermal energy made the casting process 50% faster than the aluminum die-casting. Material fabricated by the die casting process contains porosity, shrinkage cavity, and macro-segregation.

1.4.1.2 Semi-solid casting

To improve the quality of the products, semi-solid casting, or the compo-casting process, was developed. This method has gotten considerable interest as a powerful manufacturing process of producing metal matrix composites. Materials prepared by the semi-solid casting process contains lower shrinkage cavity, small amount of macro-segregation, and less amount of entrapping mold gases compared to conventional die casting [14, 15]. In the conventional die casting method, incorporation of ceramic particles in a metal matrix is difficult because of lack of wettability between molten metal and ceramic reinforcements. On the other hand, uniform distribution of ceramic reinforcements in the metal matrix is obtained by mechanical mixing in a semi-solid process.

Casting of metal matrix composites using semi-solid processes were first investigated in the early 1970s [16]. In those methods, the non-wetted ceramic particles were mechanically trapped, vigorously stirred in the partially solidified slurry of alloys to prevent the floating and settling of the particles in the melt.

1.4.1.3 Squeeze casting

The concept of squeeze casting was introduced in the early 1800s [17, 18]. However, the application of squeeze casting was first observed in 1931 [19]. SiC_w/Mg [20], SiC_w/ AZ91 [21] and many other Mg matrix composites were prepared using this method. Fig. 1.2 shows the steps involve in the squeeze casting process. In the squeeze casting method, prefabricated preforms are prepared by reinforcing particles or short fibers without adding binders [22]. Then, the preforms are heated at a certain temperature to avoid solidification at the time of infiltration of Mg melts into the preform. Mg is also heated at a temperature higher than its melting temperature and it is poured into the preheated preforms. After that, high pressure is applied to solidify the mixture of Mg melt and preform. The effect of pressure gives equiaxed microstructure having no porosity and no residual gases. Squeeze casting allows using high volume fractions (~ 40-50%) of reinforcements [23]

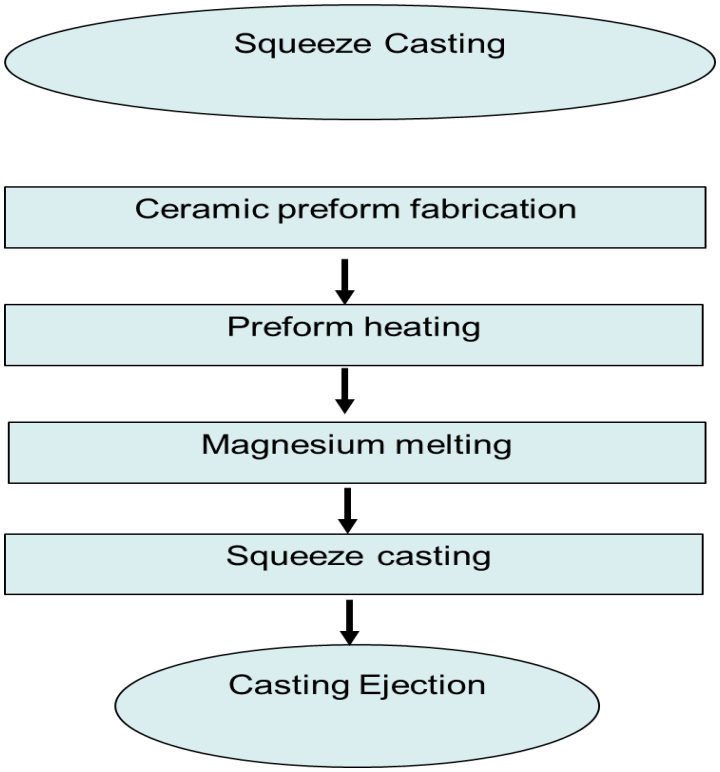

Fig. 1.2 Squeeze casting technique to fabricate Mg matrix composites [23]

1.4.1.4 Stir casting

Among various metal matrix composite methods, stir casting is accepted as a promising manufacturing route due to its simplicity, flexibility and capability of producing large amounts of bulk composites [24]. It also minimizes the final cost of the product by allowing the conventional metal fabrication technique. This method allows the fabrication of large parts and complex structures.

Fig.1.3 describes the steps involved in the stir casting process [25]. Mechanical stirring in the furnace is the primary factor that affects the fabrication method. The short fibers or particles are mixed with the molten matrix with the aid of a mechanical stirrer. Then the resultant molten material can be fabricated by die casting, sand casting or permanent mold casting. The mechanical stirrer helps the distribution of reinforcements in the composites, and a uniform distribution can be obtained by controlling the stirring time. In the stir casting process, the amount of reinforcement can be reached up to 30 Vol. % of the composites [26]. Several numbers of Mg matrix composites were prepared using this method such as 15SiC/Mg-Al9Zn, 15SiCp/Mg-Zn5Zr [27], SiCp/Z6 (Mg - 6 % Zn), SiCp/AZ31B [28], SiCp/pure Mg [29], SiCp/ ZC63 [30].

However, the poor wettability between the particles and the liquid matrix, and floating of the reinforcements are the major drawbacks of this method. Porosity due to shrinkage of the molten metal and the un-known chemical reactions between the matrix and the reinforcement are also the considering factors of using the stir casting method.

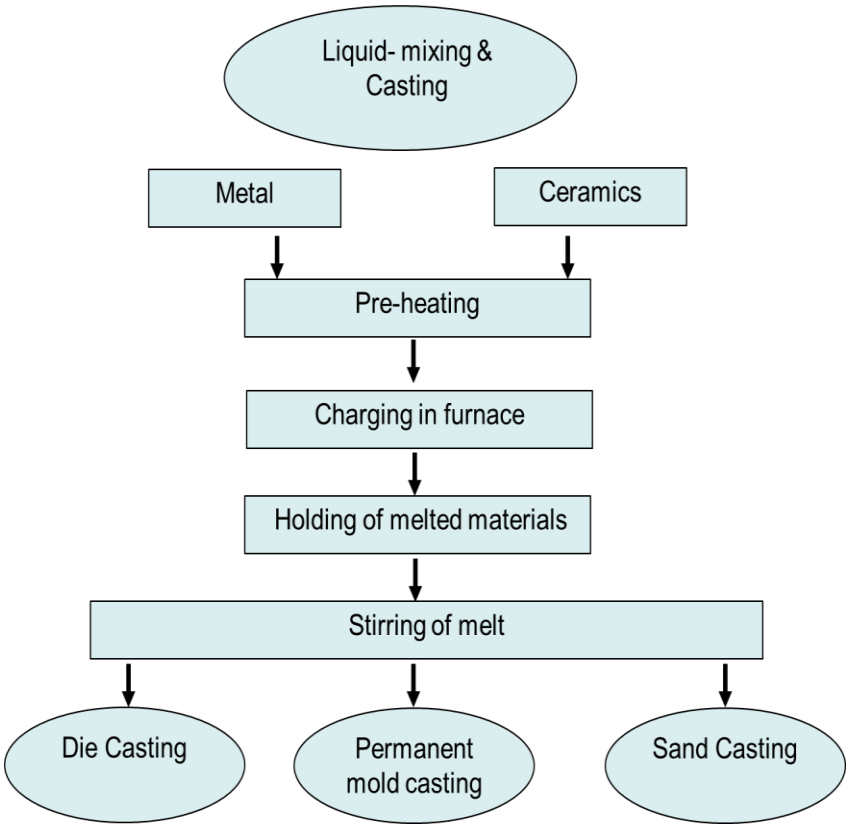

Fig. 1.3 Schematic diagram showing stir casting process [25]

1.4.2 Spray processing

The spray forming process was invented by Singer in 1985 [31]. In this method, the atomized streams of molten ceramic particle droplets were deposited onto a matrix substrate. The typical average droplet velocities were 2-40 m/s [32]. MMC materials produced in this process showed homogeneous distribution and the porosity was about 5-10%.

Fabrication of Mg matrix composites using the spray forming process, process parameters, and microstructure and mechanical properties were analyzed by several studies [14, 33, 34]. From the studies on processing parameters, it was found that rapid solidification played

an important role in the fabrication of SiC (8-12μm) particles reinforced QE22 (Mg alloy) matrix composites [33]. Mechanical characterization showed that after rapid solidification using this method, the ductility was significantly improved, whereas the ultimate tensile strength and yield strength were improved moderately compared to conventional casting methods.

SiC reinforced Mg-10% Ce and Mg-5% Ca alloy matrix composites were successfully prepared by Noguchi *et al*. using spray deposition process. They reported that the relative density was higher than 95% after simultaneous injection of SiC particles [35]. The uniformity of distribution of SiC particles were improved after hot extrusion and the relative density was above 99% in the case of extruded samples. SiC particle having diameters less than 1 μm was also dispersed successfully using this process. Mechanical characterization showed an improvement in hardness and elastic modulus after reinforcement of SiC particles. However, the tensile strength was not improved in this process. The cost of composites fabricated by Spray processing were between the powder processed composites and material synthesized by the mixing method.

1.4.3 Disintegrated melt deposition technique

DMD techniques combine the advantages of spray processing and die casting techniques [36]. Fig. 1.4 shows the schematic diagram of disintegrated melt deposition method. This hybrid method involves the superheating of the mixture of metal matrix and reinforcements in a crucible under inert gas atmosphere. The molten slurry is then stirred using a twin blade mild steel impeller to facilitate the uniform distribution of reinforcements in the matrix. After that, the melt is released through an orifice at the base of the crucible. The resulting composite slurry is then disintegrated by two jets of argon gas oriented in the direction of normal to the melt stream. Subsequently, the molten slurry is deposited onto a substrate. Compared to the conventional spray processing method, the DMD process employs higher superheating temperature and lower impinging jet speed.

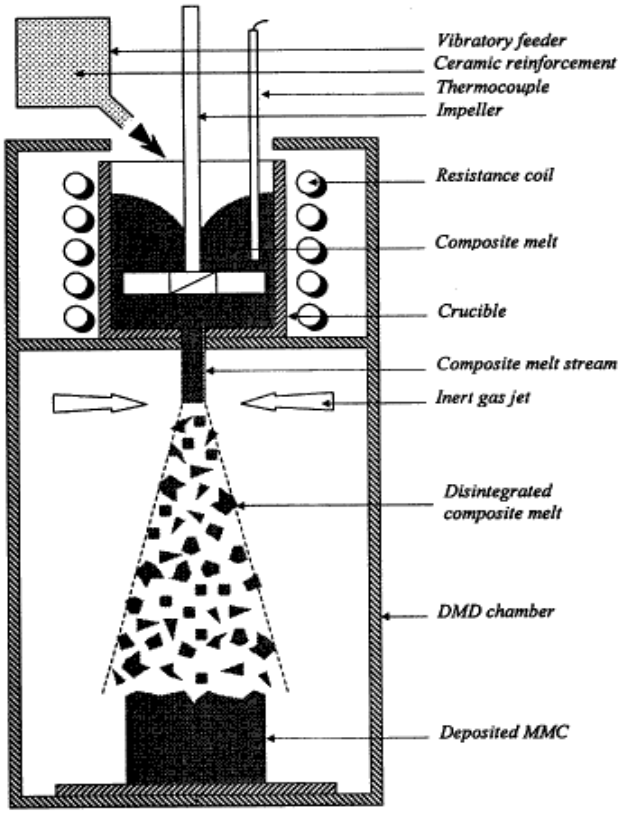

Fig.1.4 Schematic diagram of disintegrated melt deposition method [36] (Reprinted with permission from Elsevier).

1.4.4 Powder metallurgy

Due to the difficulty of wetting ceramic particles in molten matrix, powder metallurgy is considered as an alternative technique. Powder metallurgy also has the advantage of better control on the microstructure compared to the casting methods [10]. A wide range of Mg matrix composites were synthesized using the powder metallurgy technique in the past, such as SiC reinforced AZ91 matrix composites [37], SiC reinforced QE22 matrix composites [38], and B_4C reinforced AZ80A (Mg alloy) matrix composites [39]. In the powder metallurgy technique, particles or fibers were mixed with the Mg or Mg-alloys using a mixer. The powders were then pressed, degassed and sintered in a controlled atmosphere [40]. To get optimum dispersion, it is necessary to control the ratio of matrix and reinforcing particles or fibers.

The powder metallurgy technique has the following advantages:

- Any alloy can be used as a matrix material
- Any type of reinforcement can be used because the unwanted reactions between the matrix and reinforcements can be controlled using solid state processes
- It is possible to incorporate high volume fraction of reinforcements. High volume fractions of reinforcement maximize the modulus and minimize the coefficient of thermal expansion
- The possibility of mixing immiscible matrix and reinforcements, which are not possible in the liquid casting method.

However, the major difficulty of this method is the complexity of the process, and it is not beneficial for mass production.

1.4.4.1 Hot pressing

Hot processing is a method to fabricate metal and ceramic materials by applying heat and pressure. By using this method, it is possible to obtain fully dense samples of ceramics and metals having controlled microstructure. Carreño-Morelli *et al.* synthesized carbon nanotube (CNT)/Mg composites using uniaxial hot pressing followed by hot isostatic pressing [41].

Before hot pressing, Mg powders and CNTs were mixed by dry blending for 4 hour in a Turbula T2C mixture. Uniform distribution of CNTs in the Mg matrix was obtained and the relative densities of the samples were up to 98%. Resonant measurements showed 9% improvement of Young's modulus of Mg-2 wt% CNTs compared to un-reinforced sintered Mg.

Mizuuchi *et al.* used pulse current hot pressing to fabricate TiNi shape memory alloy reinforced AZ31 (Mg alloy) composites [42]. AZ31 plates with 20 vol% of TiNi alloy were hot pressed at a consolidation temperature of 500° C for a total holding time of 0.3 ks with a heating

rate of 1.7° C/s. TiNi reinforcements improved the yield stress of AZ31 alloy 105% at 150°C and 55% at 100°C.

1.4.4.2 Hot isostatic pressing

In the hot isostatic pressing process, isostatic gas pressure is applied in addition with high temperature inside of a vessel. Usually very high pressure is applied to consolidate powders in case of hot isostatic pressing. Argon is mostly used as the pressurizing gas. Ye *et al.* investigated Ti6Al4V/AM60B matrix composite fabricated by melting followed by hot isostatic pressing [43]. Microstructure characterization revealed the uniform distribution of Ti6Al4V particles in the matrix and the presence of a minimal amount of porosity. However the presence of Ti6Al4V did not produce any beneficial effect on the room temperature tensile strength and it reduced the ductility of the composite. Ti6Al4V/matrix interfaces might act as preferred sites for the void formation and crack propagation, and poor bonding between the reinforcement and matrix was observed.

1.4.4.3 Spark plasma sintering

Spark plasma sintering (SPS), also known as pulse electric current sintering, is a novel nanoprocessing method where uniaxial pressure and pulse direct current are applied simultaneously. SPS gives full densification of metal matrix composites with a relatively shorter sintering time and lower temperature compared to other densification processes. The detail about spark plasma sintering is discussed in the next section.

1.5 Role of spark plasma sintering process parameters

The primary features of Spark Plasma Sintering include a high heating rate, the effect of uniaxial pressure and the effect of electric current. High heating efficiency is obtained and high quality

sintered samples having clean grain boundaries, homogenous microstructure, and lower oxidation content can be produced [44].

Recently, electric current is widely used to activate the sintering process due to commercial availability of electric devices but the origin of its use to enhance sintering is seven decades old [45]. Uses of electric discharges to assist sintering of powders were described by earlier patents in 1933 [46, 47]. These patents demonstrated the effect of electric current for heating during the wielding process and sintering of hard particles. Later works on sintering using electric current which is known as "Spark Sintering" was done in 1960's and 1970's by Inoue *et al*. [48-50]. Before this, different groups called these types of sintering processes as plasma assisted sintering (PAS), pulsed electric current sintering (PECS), electro-consolidation which is also known as electric pulse assisted consolidation (EPAC), pulse discharge sintering (PDS), resistance sintering (RS), pulse current sintering (PCS), field activated sintering technique (FAST) by different groups . Today, it is called as spark Plasma Sintering (SPS).

Fig. 1.5 describes the mechanism of spark plasma sintering [51]. Initially, the powders are put into the die (graphite or metallic). The powders must be either electrically conductive or isolating for this process. Then the powders are initially activated by passing current (usually pulse direct current) through the die, punches and powders. After obtaining a certain activation level by the pulse direct current, the powders are consolidated using uniaxial pressure. The sintering process has three stages [52]. These stages are

- The first stage is known as plasma heating. The electric charge between the powder particles results in localized heating. A high heating rate up to several thousand ºC can be obtained at the particle surfaces. The generated heat is uniformly distributed as the micro-discharges form uniformly throughout the samples. Impurities on the particle surfaces are vaporized and

the purified surface layers are activated. The melting and fusion of the purified surface layers to each other forms “bridge or neck” between the particles.

- At the second stage the pulse direct current passes from particle to particle through the bridges between them. Joule heating is generated due to this electric current. Joule heating increases the diffusion of the atoms / molecules between the particles through these necks.

- The final stage involves plastic deformation of the heated materials under uniaxial pressure. High densification is obtained due to the combined effect of diffusion and plastic deformation.

In SPS, the consolidation of the material is done under the simultaneous effects of current and pressure. The characteristic parameters of SPS include a) heating rate b) the effect of pressure and c) the application of the current

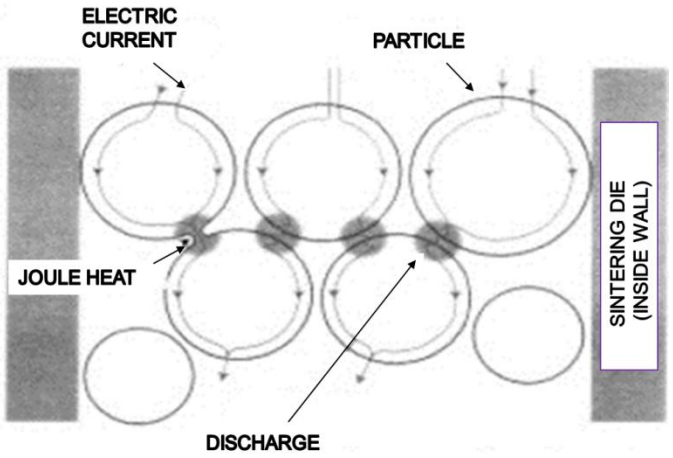

Fig. 1.5 Schematic showing spark plasma sintering mechanism [51] (Reprinted with permission from Elsevier)

1.5.1 Effect of heating rate

The primary difference between conventional Hot-pressing and SPS is the heating rate. SPS allows working at heating rates as high as 1000° C/min [53]. Joule heating occurs at the powders and the interfaces, and due to this Joule effect higher heating rate is obtained. Heat transfer also occurs between the dies and punches through powders.

The effect of heating on sintering was studied in the cases of pressure-less sintering and pressure assisted sintering [45]. Higher heating rate in pressure-less sintering creates a large thermal gradient that by passes the lower temperature stages. The higher temperature gradient creates an additional driving force for sintering. This driving force intensifies sintering of the particles. The lower temperature zone is responsible for the non-densification mechanism of surface diffusion.

Several studies were conducted to analyze the effect of heating rate on densification and grain growth of materials. However, these studies reported conflicting conclusions about their results. Two different types of powders, Al_2O_3 (insulating) and $MoSi_2$ (electrically conductive), were sintered using heating rates between 50° C/min and 700° C/min [54]. It was found that heating rate does not have any effect on the densification behavior of these materials. However, Al_2O_3 showed an inverse relationship between the grain size and the heating rate. $MoSi_2$ did not show any heating rate effect in case of grain growth. Zhou *et al.* [55] investigated the effect of heating rate on the densification behavior of Al_2O_3 particles. Heating rate between 50° C/min and 300° C/min did not make any significant difference on the final density of Al_2O_3 but grain size significantly reduced with increasing heating rate. Shen *et al* .[56] also investigated the effect of heating rate on the grain size and densification behavior of Al_2O_3 particles of in the heating rate range of 50° C/min to 600° C/min and obtained conflicting results. Heating rate had little effect on the densification of alumina particles up to 350° C/min but after that the relative density started to decrease significantly with the increment of heating rate up to 600° C/min. However the

grain size significantly decreased with the increment of heating rate up to 200° C/min and after that it had little effect on grain size. Anselmi-Tamburini *et al.*[57] studied the effect of process parameters of SPS on the densification behavior and grain growth of fully stabilized zirconia nano-powders and found no significant influence of heating rate (in the range of 50-300° C/min) on the final density and crystalline size of zirconia nano-particles.

1.5.2 Effect of pressure

When powders are sintered under the application of uniaxial pressure, higher densification is obtained at the same sintering temperature. The effect of pressure breaks agglomerations and re-arranges the particles; especially in the case of nano-particles [45]. It also breaks the nascent oxygen presents in the particles. The effect of pressure can be described by the driving force for sintering [51]:

$$\frac{d\rho}{(1-\rho)dt} = B\left(g\frac{\gamma}{x} + P\right) \ldots\ldots\ldots\ldots\ldots\ldots\ldots\ldots\ldots\ldots\ldots\ldots\ldots\ldots\ldots\ldots\ldots\ldots\ldots\ldots\ldots\ldots\ldots\ldots .. (1)$$

Where, ρ = fractional density

B= Constants includes diffusion co-efficient and temperature

g = geometric constant

γ = surface energy

x= Constant that is related with particle size

t= time

P= External applied pressure

The first term of the right hand side of equation (1) represents intrinsic driving force for sintering while the second terms represents the intrinsic effect of applied pressure to the driving force. The point at which these two contributions will be equal is presented by

$$P = g\left(\frac{\gamma}{x}\right)\ldots\ldots\ldots\ldots\ldots\ldots\ldots\ldots\ldots\ldots\ldots\ldots\ldots\ldots\ldots(2)$$

Skandan *et al.* [58] studied the effect of applied pressure on the densification behavior of nanoparticles of ZrO_2. From their investigation, it was found that there was a threshold pressure below from which there was a little contribution of applied pressure over the densification behavior. In the case of fine-grained particles (6 nm), the threshold value was 35 MPa. The density increased extensively when the applied pressure was more than 35 MPa. In case of large grained powders (12 nm), the threshold pressure was 10 MPa. Fig. 1.6 shows the effect of applied pressure on the required sintering temperature to get 95% relative density of zirconia (ZrO2) nano-powders where holding time was 5 minutes [45]. The temperature needed to get 95% relative density decreases linearly with the increment of applied pressure. The grain size decreased from 200 nm to 115 nm when the pressure was increased from 25 MPa to 800 MPa.

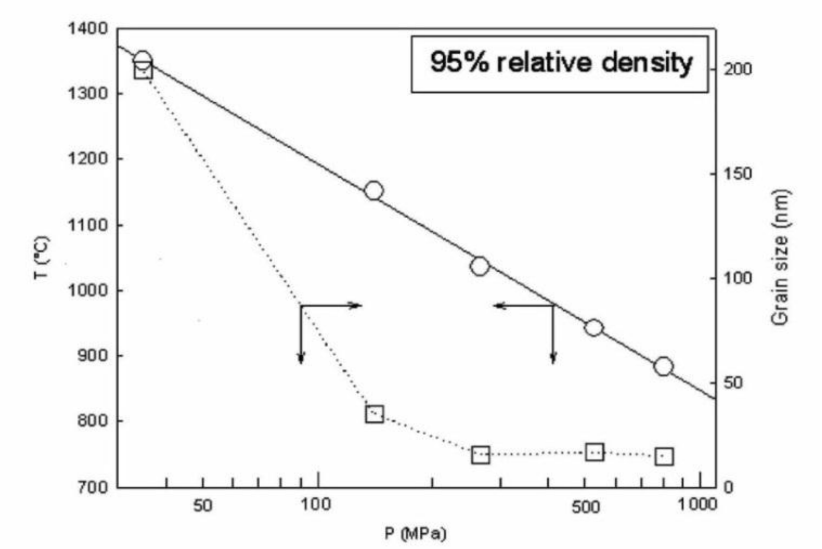

Fig. 1.6 Effect of pressure on the temperature required to achieve 95% density and grain size for ZrO_2 [45] (Reprinted with permission from Elsevier)

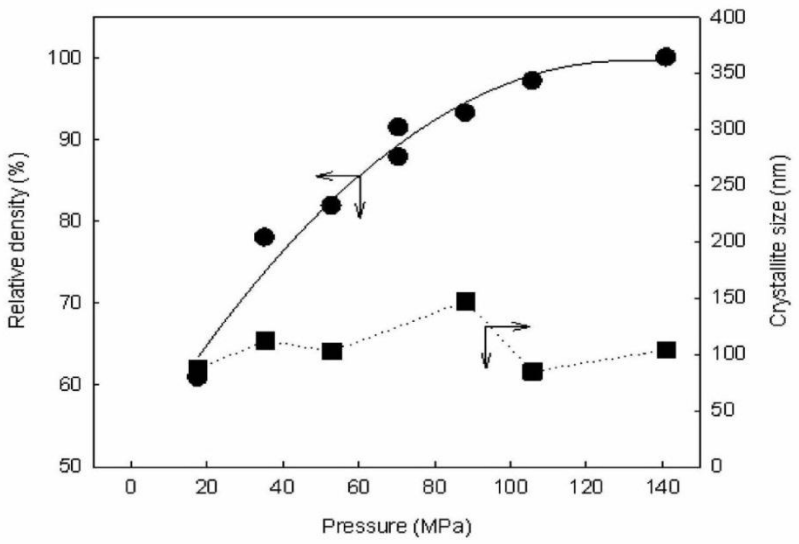

Fig. 1.7 Effect of applied pressure on relative density and grain size of cubic ZrO_2 [45] (Reprinted with permission from Elsevier)

Fig. 1.7 shows the effect of applied pressure on the relative density and crystalline size when the sintering temperature was constant in case of another type of ZrO_2 powders [45].The uniaxial pressure had no effect on the crystalline size but the relative density increased with the increment of applied pressure.

1.5.3 Effect of electric current

The major difference between the conventional hot pressing and SPS method is the effect of heating rate which is directly related with the electric current. Generally, in hot-pressing system the sample and the die are heated from the radiation which comes from an enclosing furnace. But in SPS method, the die and the sample are heated by current passing through them, which creates Joule heating. However, instead of providing only heating effect, the pulse DC current is also creating plasma which cleanses the surface of the particles. The cleansing of the particles leads to the enhancement of sintering. The effect of electric field or current on the sintering behavior has been investigated by several researchers [59-62]. From the investigation of Zhang *et al.*, it was

revealed that the presence of electric current affect the migration of defect sites, grain growth, phase transformation, diffusion etc. [59]. Applying both pressure and electric current could significantly enhance the densification of ceramic particles. In the case of densification enhancement, the pulse electric current is more beneficial compared to the steady-state electric current. Omori [50] observed that the presence of electric current breaks the surface film of aluminum and pure tungsten carbide powders. However, the influence of current was debated by some other researchers [60-62]. Wang *et al.* [61] did not observe the effect of pulse direct current. Ozaki *et al.* [63] sintered aluminum powders and did not find any presence of discharge even after using conducting graphite die.

1.6 Mg based composites: a review

Researchers tried to fabricate different Mg-matrix composites using various fabrication methods. Different contents of reinforcing material were also used. In this section, fabrication and characterization of different types Mg matrix composites are described.

1.6.1 Ceramic particle reinforced Mg matrix composites

Ceramics are the most common reinforcements in metal matrix composites. Due to the excellent intrinsic properties of ceramic materials, they are desirable for reinforcement in Mg matrix. Ceramic materials have very high hardness, excellent strength, excellent elastic modulus and very good thermal conductivity. However, they have some limitations such as low wettability, very low ductility and low compatibility with Mg matrix. Widely used ceramic reinforcements are SiC, Al_2O_3, TiC, Y_2O_3, SiO_2 etc. Among these reinforcements, SiC and Al_2O_3 are well known. Even though the improvements of mechanical properties are inferior compared to the fiber reinforcements, they are considered to be advantageous in terms of cost, processing and some other properties such as the compressive strength. Particulate reinforcement provides improvement in properties including improved wear and erosion resistance, higher stiffness,

better damping properties and lower thermal expansion coefficient compared to the un-reinforced metals and alloys.

1.6.1.1 Al_2O_3 reinforcement

Al_2O_3 exhibits good mechanical properties at high temperatures, excellent specific stiffness, and good oxidation resistance [64, 65]. Hassan *et al.* reported fabrication of Al_2O_3 reinforced Mg-based composites using disintegrated melt deposition (DMD) technique coupled with hot extrusion [66]. Three different sizes of Al_2O_3 particles (ranging from nanometer to micrometer scale) were used as the reinforcements. The content of the Al_2O_3 particle was 1.1 Vol. %. Microstructural characterization showed the uniform distribution of Al_2O_3 particulates in the Mg-matrix with strong interfacial bonding and notable reduction of grain sizes. Mechanical characterization revealed that the Al_2O_3 particulates in Mg matrix showed simultaneous improvement in hardness, 0.2% yield strength, ultimate tensile strength and the ductility of pure magnesium. It was also revealed that the nano-size particles were more effective than the micro-particles in increasing the combination of hardness, strength and ductility.

Using DMD technique, alumina particle (having particle size of 50 nm) reinforced AZ31B (magnesium alloy) matrix composites were also synthesized by Nguyen *et al.* [67]. DMD technique was followed by hot extrusion at a temperature of 350° C. SEM images of the composites revealed equiaxed grain structure, small amount of porosity, good interfacial bonding and uniform distribution of Al_2O_3 nano-particles. Mechanical characterization showed improvement in microhardness and ductility of the composites compared to the un-reinforced alloy. However, the decrement of both 0.2% yield stress and ultimate tensile strength revealed the incapability of alumina nano-particles to act as obstacles to dislocation movements. The same materials were analyzed to reveal the compressive response [68]. Compression testing of the

composites showed improvement in 0.2% compressive yield strength, ultimate compressive strength and strain at failure of the composites compared to the un-reinforced alloy.

Stir casting method was used to fabricate 0.5 wt. %, 1 wt. % and 2 wt. % alumina reinforced Mg and AZ31 magnesium alloy matrix composites by Habibnejad-Korayem *et al.* [69]. The particle size of the alumina particles were 100 nm. Microstructural characterization showed a uniform distribution of alumina nanoparticles in the matrix. Al_2O_3 nano-particles also refined the grains and decreased the coefficient of thermal expansion which improved the dimensional stability of the matrix. Mechanical characterization showed the improvement of hardness, 0.2% yield strength and ultimate tensile strength with the increase of alumina content. These properties reached their maximum when the alumina content was 2%. However, this caused a significant amount of reduction in the ductility of the composites compared to the pure Mg and AZ31 alloy. The primary contribution for the improvement of 0.2 % yield strength was CTE mismatch between the matrix and the reinforcement. The secondary contribution was from Orowan strengthening, grain refinement and the load bearing effect of Al_2O_3 nano particles. The reduction of ductility was attributed as the change of fracture mood from quasi-cleavage fracture mood to an advanced brittle state. This was revealed by the SEM images of the fractured surfaces.

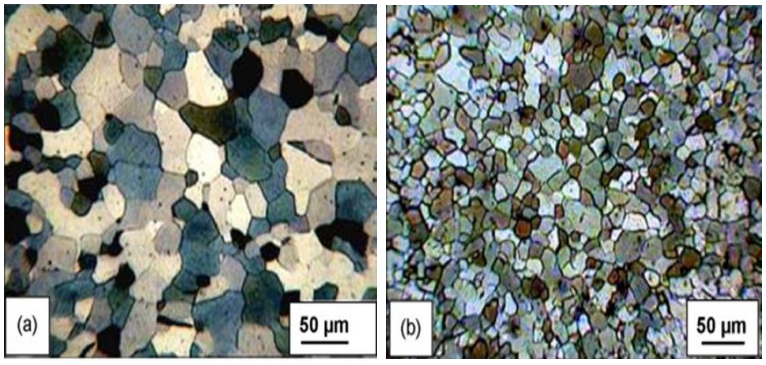

Fig. 1.8 Optical micrographs of (a) pure Mg, and (b) Mg-Al_2O_3 wrought materials [69] (Reprinted with permission from Elsevier)

1.6.1.2 TiC reinforcement

In general, TiC has very poor wettability in contact with magnesium, and an un-known interfacial reaction occurs when the composite is synthesized using ex-situ methods [70]. In-situ techniques are usually used to fabricate TiC reinforced magnesium matrix composites. Jiang *et al.* synthesized TiC particle reinforced AZ91 matrix composites by adding TiC-Al master alloy using the semi-solid slurry stirring technique [70]. In the master alloy, TiC particles were in situ formed in Al via self-propagating high temperature synthesis (SHS) reaction. As the TiC particles were surrounded by the Al particles, the surfaces of the TiC particles remained un-contaminated and good wettability of TiC particles in the magnesium matrix was observed. The UTS, hardness and wear resistance of TiC reinforced Mg matrix composites were better than that of un-reinforced magnesium alloy matrix.

1.6.1.3 SiC reinforcement

Silicon Carbide acts as a promising reinforcing material in metal matrix composited due to its tailorable mechanical properties such as high hardness and strength. Large number of studies have been conducted about micro-SiC particle reinforced Mg-matrix composites. Submicron SiC particle (0.2μm) reinforced AZ91 matrix composites were prepared using stir casting method by Deng *et al.* [71]. The as cast ingots were forged, extruded, and mechanically tested. Microstructure characterization showed a uniform distribution of SiC micro-particles, grain refinement, and the presence of a small amount of porosity. Both the 0.2% yield strength(YS) and ultimate tensile strength (UTS) started to increase with the increment of SiC content and reached their maximum when the SiC content was 2 Vol.%. After this amount of reinforcement, the 0.2% YS and UTS started to decrease due to the agglomeration of SiC particles. But the micro-hardness and elastic modulus continuously increased with the addition of SiC submicron particles.

It is believed that nano size SiC particles would give enhanced properties even after the addition of a small volume fraction of reinforcement. Previous studies reported that nano-SiC gives better grain refinement compared to micro size SiC reinforcement in Al matrix [72].

Ferkel *et al.* again used the powder metallurgy method to fabricate SiC nano-particle reinforced magnesium matrix composites [73]. 3 Vol% SiC nano-particles (having particle size of 30 nm) were mixed with Mg particles (having particle size of 40μm) for 8 hours at 200 rpm using an asymmetrical moved mixer. Then, the powders were ball milled for 8 hours in a planetary ball mill. Next, the composite powders were encapsulated in a vacuum container, degassed and extruded at a temperature of 350°C. For comparison purposes, pure Mg was also fabricated in the same way. Light optical microscopy showed the average particle size of 20μm for pure magnesium and 1 μm for Mg-3% nano SiC samples. The milled Mg-3% nano SiC exhibited lower creep rates and large flow stress compared to the pure Mg.

Nano-SiC reinforced Mg-matrix composites were prepared by casting with the aid of high-intensity ultrasonic cavitation method by Jan *et al.* [74]. 2 wt. % and 5 wt. % of nano-SiC, having an average diameter of 30 nm were mixed with AZ91D alloy with the help of an ultrasonic transducer. High resolution SEM images showed a nearly uniform distribution and good dispersion of SiC particles in the composite. But some clusters (less than 300 nm) were also present in the AZ91 D matrix. EDS analysis showed the presence of Mg_2Si which was due to the partial oxidation of SiC nanoparticles. The micro-hardness value increased with the increment of SiC contents and it reached an improvement of 75% after the addition of 5 wt. % SiC particles compared to pure AZ91D alloy.

Again, ultrasonic cavitation technique was used to disperse 2 wt. % nano-SiC particles (having an average size of 50 nm) in the Mg-(2,4)Al-1Si magnesium alloy melts by Gao *et al.* [75]. The ultrasonic probe was dipped in the molten alloy containing SiC nano-particles. To produce the tensile specimens, the melt was cast in a permanent mold. Compared to the

unreinforced alloy, the tensile strength and yield strength of the SiC reinforced Mg-alloy composites were improved significantly while the ductility of the nano-composites retained. SEM images showed the presence of some clusters of SiC in the material. These clusters occurred mainly at the grain boundaries while most separated nano-particles were embedded inside the grains. The improvement of mechanical properties was attributed to the uniform distribution of nano SiC particles, the grain refining and strengthening effect of dispersed nano-particles. It was also found that some of the Si particles reacted with Mg and forms Mg_2Si in the matrix.

1.6.2 Carbon allotropes reinforced Mg matrix composites

Recently, some of the carbon allotropes gained attention due to their mechanical, electrical and thermal properties. Researchers have tried to incorporate the carbon allotropes in Mg matrix. Most common carbon allotropes are carbon nanotubes and graphene.

1.6.2.1 Carbon nanotubes

Carbon nanotubes (CNTs) exhibit a good combination of electrical and thermal conductivities, and mechanical strength. Significant efforts have directed towards using the advantageous properties in a wide range of applications, including those of structural, electronic and energy applications [76, 77].

Various liquid and solid state processing methods were used to fabricate the CNTs reinforced magnesium metal matrix composites [78- 82]. MWCNT/ AZ31 composites were prepared by Morsida *et al.* using the friction stirring process [78]. The length of the CNTs were 250 nm and the outer diameters were 20-50 nm, whereas the AZ31 powder was rolled plates having a thickness of 6 mm. MWCNTs were randomly distributed in the AZ31 matrix using this method. Maximum hardness was 78 HV due to the presence of nanotubes and grain refinement effects whereas the hardness of AZ31 was 55 HV.

Pure Mg reinforced with 0.3%, 1.3%, 1.6% & 2% CNTs were prepared using the disintegrated melt deposition (DMD) method [79]. The nano-composites were extruded at a temperature of 350°C. In order to compare the properties, Mg samples were also fabricated and processed in the same way. A small amount of increment of hardness was achieved in case of Mg-0.3% CNT composite. The hardness value started to drop after this amount of CNT reinforcement. Simultaneous improvement of yield strength, ultimate tensile and ductility was achieved for Mg-CNT composites fabricated by Goh *et al.* and reached a maximum in the case of Mg-1.3% CNT. Ductility improvement was due to the initiation of prismatic slip plane and the high activity of the basal slip system [80].

A two- step process was designed and applied to fabricate the CNTs/Mg alloy composites by Li *et al.* [81]. In the first step, the carbon nanotubes were dispersed into the AZ91 alloy chips using a block copolymer which acted as a dispersion agent. In the next step, MWCNT coated Mg chips were fabricated using the melt stirring technique and a good dispersion was obtained. After addition of small percentage of CNTs, the mechanical properties improved significantly. Compared to un-reinforced AZ91 alloy, AZ91-0.1wt% MWCNT gave 36% improvement in the compression at failure, 10% improvement of 2% yield strength and 20% improvement of ultimate compressive strength.

The ultrasonic vibration method was used to disperse un-bundled CNTs in the pure Mg-matrix composites by Kondhoh *et al.* [82]. To obtain the uniform dispersion in the matrix, Zwitteronic solution was used. The solution of Mg and CNTs was dried and in the next step the fabrication of Mg/CNTs composites were prepared using the spark plasma sintering method in order to prevent re-agglomeration. SEM images of dried powder showed the CNT coated magnesium particles (Fig. 1.8). 25-40% improvement of tensile strength was obtained after the addition of 1% CNTs. However, extreme decrease of ductility was found in the case of Mg-CNTs

composites. The poor ductility can be attributed to the presence of high amount of MgO in this process.

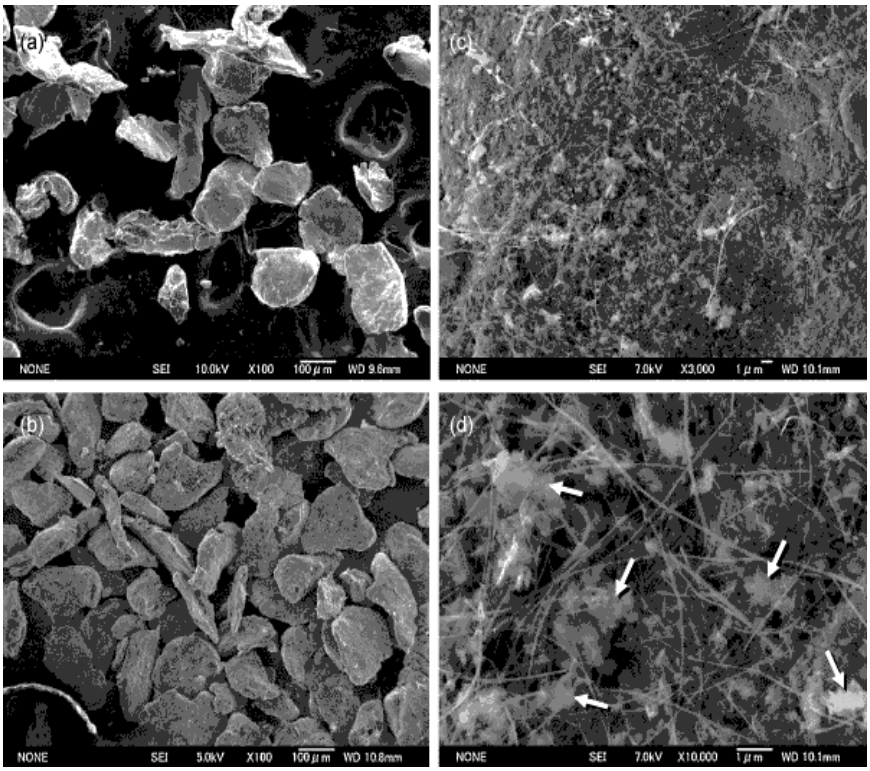

Fig. 1.9 SEM images of (a) pure Mg powders, and (b-d) Mg powders coated with CNTs after drying at 80° C in atmosphere. Arrows indicate some surfactants in the form of solid [81] (Reprinted with permission from Elsevier)

1.6.2.2 Graphene

Graphene has attracted attention as a desired reinforcement due to its excellent properties, such as high Young's modulus, high strength, extreme thermal, and electrical conductivity [83, 84]. Reinforcement of graphene platelets have been extensively analyzed in the case of polymer matrix and ceramic matrix composites [85-95]. Graphene has been reinforced in the form of single layer graphene platelets (GPL), multi-layer GPL, and graphene nano-sheets [96]. However, a limited number of studies have been conducted about graphene reinforced metallic composites.

The main reasons behind these limited studies are the extreme difficulties in dispersion of Graphene in metal matrix composites and unpredictable interfacial reactions between metals and platelets.

Chen *et al.* studied graphene nano platelets reinforced magnesium matrix composites using a combination of liquid state ultrasonic processing and solid state stirring method and achieved improvement in micro-hardness value [97]. However, no study was conducted about Graphene nano platelets reinforced Mg-matrix composites using spark plasma sintering method and the effect of GPL reinforcement in the wear properties of these composites.

1.8 Objectives

- Fabrication of Mg-GPL and Mg-nano SiC composites using ball milling and spark plasma sintering technique
- Microstructural characterization of Mg-GPL and Mg-nano SiC composites
- Mechanical and Tribological characterization of Mg-GPL and Mg-nano SiC composites

CHAPTER II

EXPERIMENTAL DETAILS

2.1 Materials

Commercially available Mg powder having purity of 99.8 % with an average particle size 44μm (supplied by Alfa Aesar, Ward Hill, MA, USA) was used as the matrix material. The reinforcing materials were multilayer graphene nano-platelets (99.6%, 5-25 nm diameter, 5-25 μm thickness) supplied by American Elements, Los Angeles, CA, USA and nano-SiC (99+% pure, <80 nm in diameter, manufactured by plasma CVD method) supplied by US Research Nanomaterials, Houston, Texas.

Table 2.1 Specifications of the materials used in this study

Materials	**Density (g/cm^3)**	**Average diameter (nm)**	**Average thickness (nm)**
Mg (matrix)	1.74	44000	-
GPL (reinforcement)	2.10	5000-25000	5-25
SiC (reinforcement)	3.22	< 80	-

2.2 Processing of the composites

2.2.1 Milling process

The milling process of Mg with reinforcements was done using a high speed vibrating ball mill. Mg with its respective reinforcement material such as graphene, and SiC were placed in a 125 ml mixing jar (made of tungsten) containing tungsten ball having 10 mm diameter (Fig. 2.1). The speed of the milling was 350 rpm and ball to powder ratio was used as 5:1. In case of Mg-GPL composites, 0.1% Polyacrylic Acid (PAA) was used as a dispersion agent. Dry ball milling of the raw powders were done for 15 minutes.

Fig. 2.1 High energy ball milling machine

Loading and unloading of powders in the cup was done inside the glove box to avoid oxidation of magnesium in case of both type of composites (Fig. 2.2). For comparison, Mg powders were also ball milled using the same milling parameters.

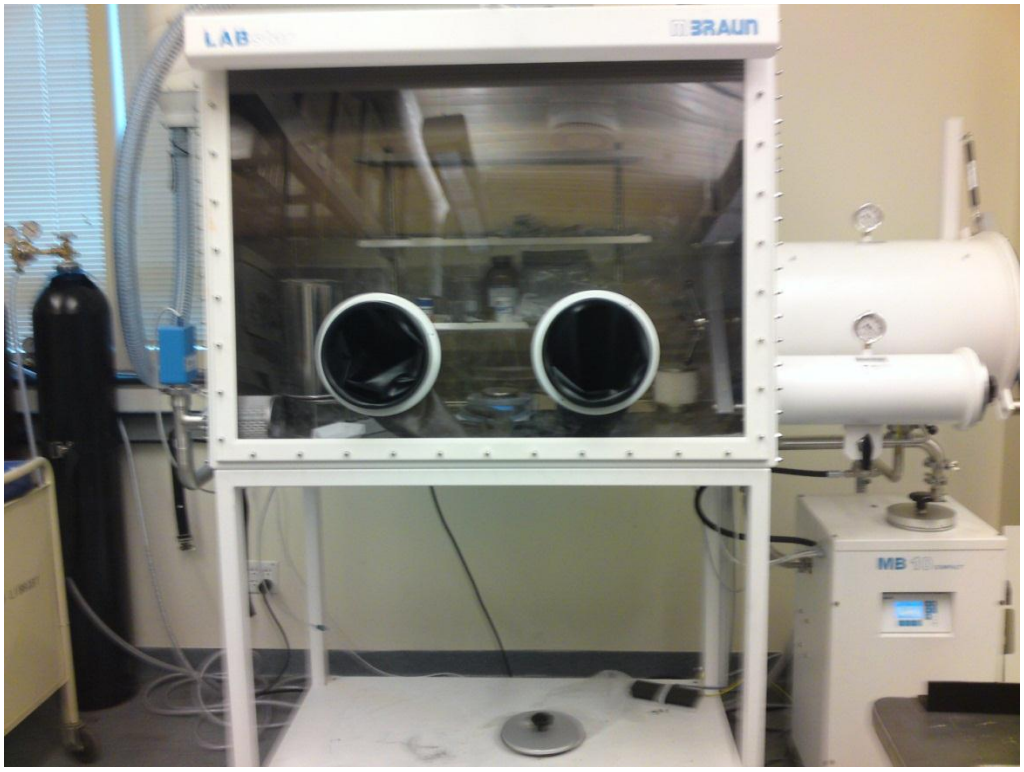

Fig. 2.2 Glove box used for handling of Mg materials

2.2.2 Spark plasma sintering

The spark plasma sintering machine (model SPS 10-3, manufactured by Thermal Technologies LLC) was used to fabricate Mg, Mg-GPL and Mg-SiC samples. Fig. 2.3 shows different parts of spark plasma sintering machine. It has 3 main parts: power unit, furnace, and cooling and vacuum pumps. This machine is capable of high heating rate up to 600° C/min. A temperature of 2500° C can be obtained within 5 minutes by using a direct current of 3000 amps and voltage of 5 V. It is also possible to get high cooling rate by purging liquid nitrogen (or liquid argon) gas in it. To avoid the contamination of powders, a high vacuum of 10^{-2} torr can be obtained at the time of sintering. When the pressure is low (≤ 100 MPa), graphite dies and punches are usually used. Graphite dies are the most widely used dies for the fabrication of spark plasma sintering as it has high thermal and electrical conductivity, and it can sustain high temperature. In our experiment, graphite dies and punches were used to sinter magnesium and magnesium matrix-composites. To

measure the temperature of the die during sintering process, K type and C type thermocouples were used.

Before fabrication of pure Mg and Mg composites, suitable sintering parameters were determined. The sintering of magnesium materials are called low temperature and low pressure sintering as the melting point of magnesium is 650° C. Powders were poured into a 20 mm diameter (inner diameter) die and powders were prepressed at a pressure of 5 MPa. Then the materials were sintered at a temperature of 450° C with a pressure of 50 MPa. The heating rate and cooling rate were maintained at 50° C/min. The holding time was kept at 5 minutes. The sintering temperature was much lower than the melting temperature of magnesium (650° C) to avoid melting. The cycles of SPS: the rapid heating from room temperature to 450° C and pressure 5 MPa to 50 MPa using a heating rate of 50° C/min and pressure raising rate of 10 MPa/min, holding time for 5 minutes at the temperature of 450° C and pressure 50 MPa, rapid cooling at a cooling rate of 50° C/min and a pressure reduction rate of 10 MPa/min.

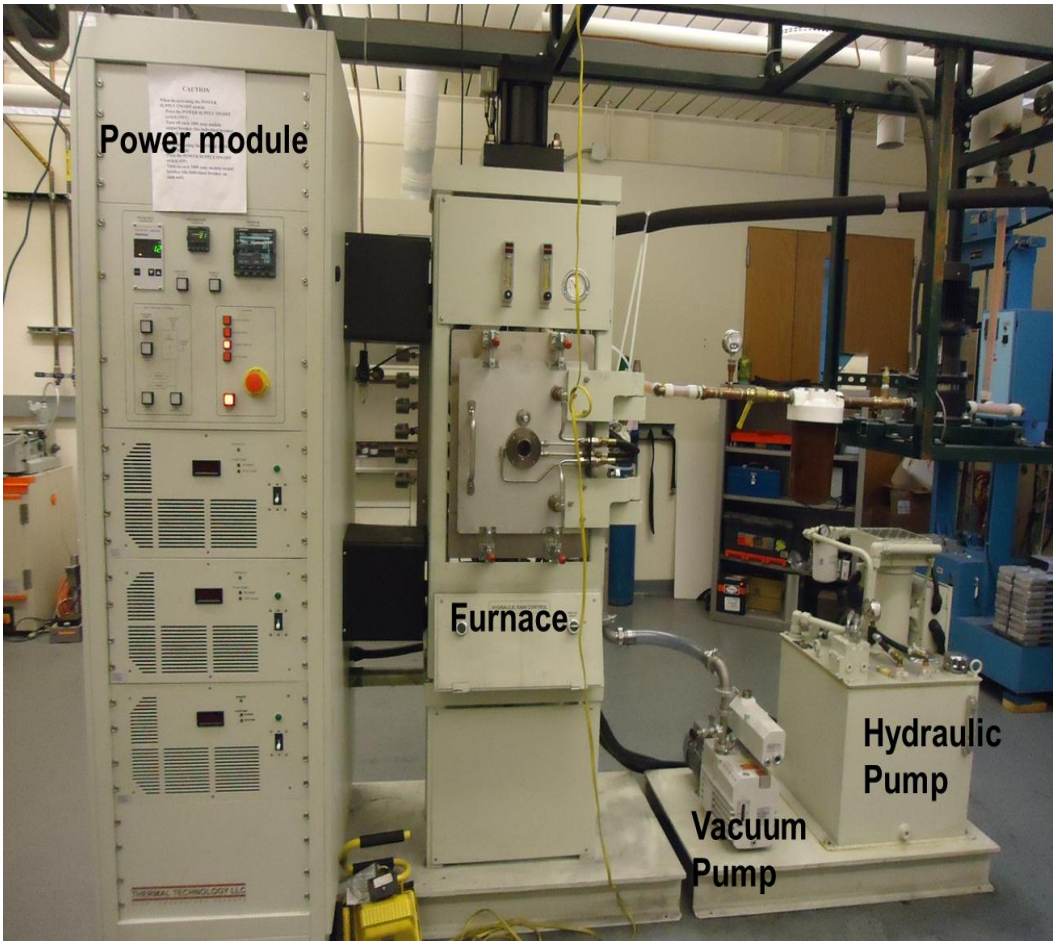

Fig. 2.3 Spark plasma sintering machine and its important components

2.3 Characterization of the composites

The samples were polished using 1200 SiC papers. For final polishing, 0.05 μm alumina powders were used to get mirror polished surface. At the time of polishing water was used as a coolant. However, small amount of distilled water was used because magnesium reacts with water and forms Mg (OH) $_2$ on the surface. After polishing, the samples were cleaned in the acetone bath using ultarsonic cleaner to remove any dust from the surface. Then the densities of the polished samples were measured.

2.3.1 Density measurement

Archimedes principle was used to measure the experimental density of the samples. Three set of readings were taken to measure the bulk density of pure Mg and Mg-composites. Average values were taken as the experimental density of the bulk samples. The samples were weighted using an analytical balance having an accuracy of ±0.0001 g and distilled water was used as immersion fluid. Theoretical densities of composites were measured using rule of mixture.

Using the Archimedes principle the experimental density was calculated using the following equation.

$$\rho = \frac{x}{x-y}(\rho_0 - \rho_L) \ldots\ldots\ldots\ldots\ldots\ldots\ldots\ldots\ldots\ldots\ldots\ldots\ldots\ldots\ldots\ldots\ldots\ldots\ldots\ldots\ldots . (3)$$

Where,

ρ = Experimental density of the sintered sample

ρ_0 = Density of the auxiliary fluid (water, at room temperature whose density is 0.99804 g/cm^3)

ρ_L =Density of air (0.0012 g/cm^3 at room temperature)

x = weight of the sample in air

y = weight of the sample in water

Relative density can be calculated as

$$\textbf{Relative density} = \frac{\text{Density of the sintered sample}}{\text{Theoritical density of the materials}} \times 100 \ldots\ldots\ldots\ldots\ldots\ldots\ldots\ldots\ldots\ldots\ldots\ldots (4)$$

2.3.2 Phase analysis

Phase analysis of Mg, Mg-GPL and Mg-nano SiC composites were measured using a Philips Norelco X-ray diffractometer operating with Cu K_α radiation (λ= 1.54178 Å) with diffraction angle(2θ) between 20° and 90° having step increment of .02°/s.

2.3.3 Microhardness testing

The microhardness of Mg, Mg-GPL and Mg-nano SiC composites were measured using a micro-hardness tester (Buehler^{TM}). The operating load was 10 g and holding time was 15 seconds. The microhardness was measured on the surfaces of magnesium and magnesium composites. At least fifteen microhardness readings were taken for each samples, and an average value with standard deviation are reported.

2.3.4 Compression testing

Compression test was done using INSTRON 5582 series universal testing machine and the strain rate was $10^{-4}S^{-1}$. ASTM E9 method was used and the aspect ratios of the compression test samples were maintained at 1 to reduce buckling effect. FEI Quanta 600 field-emission gun Environmental SEM (JSM-6360, JEOL) was used to analyze the fractured surfaces of the samples.

2.3.5 Wear testing

Ball and disk wear testing was performed using Nanovea Tribometer in the air under un-lubricated condition (Fig. 2.4). Alumina ball was used as the counter material and the diameter of the ball was 6 mm. Applied load was 1 N and the diameter of the wear track was 4 mm. The weight loss was calculated after 10 minutes interval and for each sample wear testing was continued up to 60 minutes on the same wear track. To check the repeatability of the results, three set of readings were taken for each samples. The surface profiles and depth profiles were

analyzed using Nanovea Profilometer (Fig. 2.5). SEM images of the wear tracks were taken to analyze the morphology of the wear track using FEI Quanta 600 field-emission gun environmental SEM (JSM-6360, JEOL).

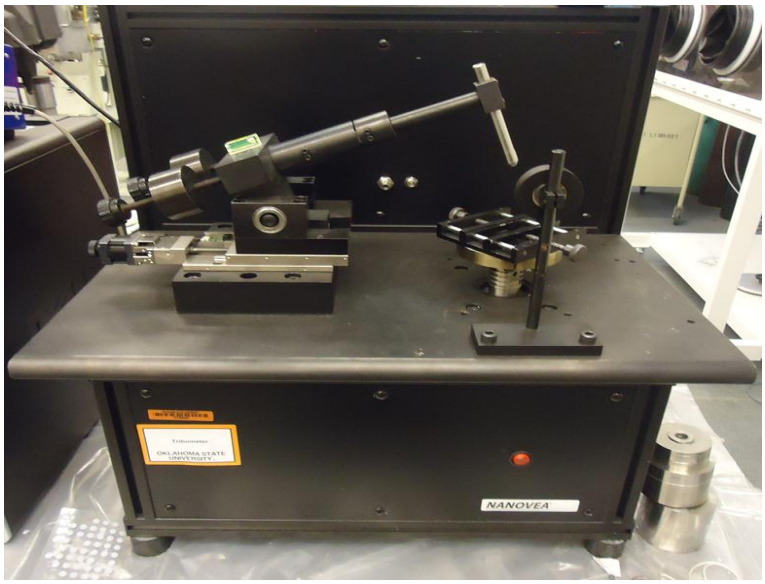

Fig. 2.4 Nanovea tribometer

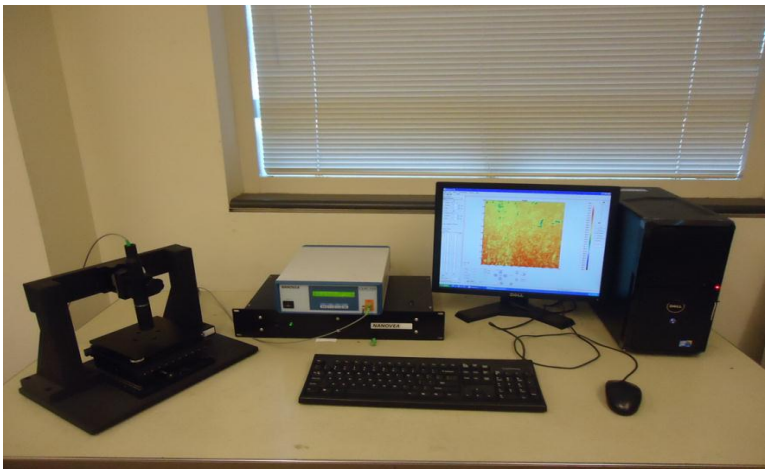

Fig. 2.5 Nanovea optical 3-D profilometer

CHAPTER III

RESULTS AND DISCUSSION

3.1 Spark plasma sintering of GPL reinforced Mg matrix composites

3.1.1 Density

Table 3.1 shows the density of pure Mg and Mg-GPL composites. It is also seen from the table that nearly full densification was obtained (≈ 98%) in case of pure magnesium sintered at a temperature of 450° C and a pressure of 50 MPa. Previous studies showed that nearly full densification (98%) was attainted in case of pure Mg sintered at 525°C using a pressure of 60 MPa [98] where the particles size of magnesium was 180 μm. In our experiments, the average particle size of pure magnesium was 44 μm. If the particle size is small then the surface area will be high. This high surface area creates high surface diffusion. High surface diffusion helps to get better density at a lower sintering temperature and pressure. Due to smaller particle size and ball milling effect, same relative density was achieved using relatively lower sintering temperature and pressure.

However, almost full densification (relative density > 99%) was observed in case of Mg-1% GPL, Mg-2% GPL, Mg-5% GPL composites. It was found that using the same sintering parameter, the relative density of Mg-GPL was higher than the pure Mg. Graphene platelets have large surface area which enhances surface diffusion at the time of sintering. As a result, Mg-GPL showed better density compared to pure Mg.

Table 3.1 Density of Mg-GPL composites

Composition	Theoretical density (g/cm^3)	Experimental density (g/cm^3)	Relative density (%)
Mg	1.74	1.70	97.58
Mg+1% GPL	1.74	1.72	99.03
Mg+2%GPL	1.74	1.74	99.82
Mg+5%GPL	1.76	1.75	99.65

3.1.2 X-ray diffraction analysis

X-ray diffraction (XRD) patterns from the spark plasma sintered Mg and Mg-GPL composites are presented in Fig. 3.1. Characteristics peak of graphene was observed at an angle (2θ) of 26° in cases of all Mg-GPL composites. Except this peak, all other peaks were Mg peaks. No peak of MgO was observed in the sintered samples. Usually, due to manufacturing short comings, MgO forms at the grain boundaries of pure Mg. If the particles get a chance to contact with oxygen again then the layer thickness of MgO will increase. As the powders were prepared inside of the glove box (oxygen content was less than 40 ppm) and both processes (ball milling, sintering) were done in argon atmosphere, the chances of oxidation was less at milling and fabrication. Previous studies showed that the sintering process decomposed the oxide layers of Ag particles, dissolved the oxide films of Cu powder surfaces and broke the stable oxide layers of Al particle surfaces [44]. Sintering process could decompose, dissolve or break the oxide layer at the surface of magnesium particles and as a result, sintered bulk samples contained small amount of MgO and no MgO peak was detected in sintered samples.

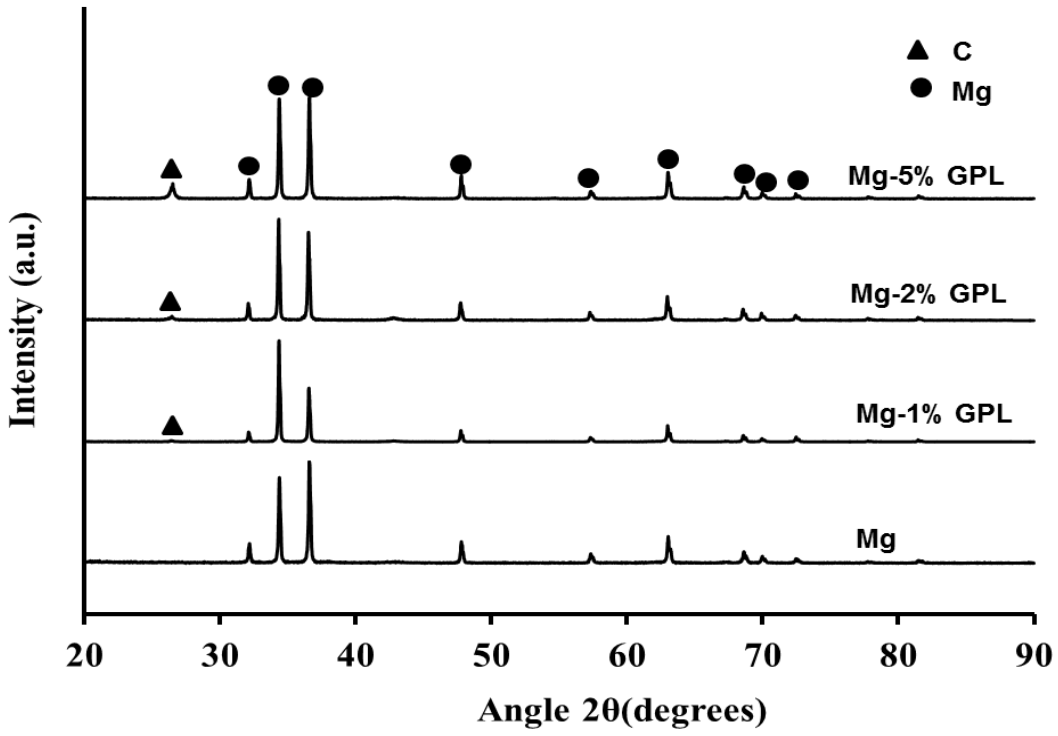

Fig. 3.1 X-ray diffraction patterns from SPS sintered Mg and Mg-GPL composites

3.1.3 Mechanical properties characterization

3.1.3.1 Microhardness testing

Microhardness values of pure Mg, Mg -1% GPL, Mg -2% GPL, and Mg-5% GPL composites are presented in Fig. 3.2. The average microhardness values of pure Mg, Mg-1% GPL, Mg-2% GPL, and Mg-5% GPL were found to be 46, 53, 63 and 49 HV by using same sintering parameters. Average microhardness values showed an incremental trend after addition of graphene reinforcement for 1% and 2%. Mg-2% GPL showed an increment of 37% hardness value compared to unreinforced Mg samples.

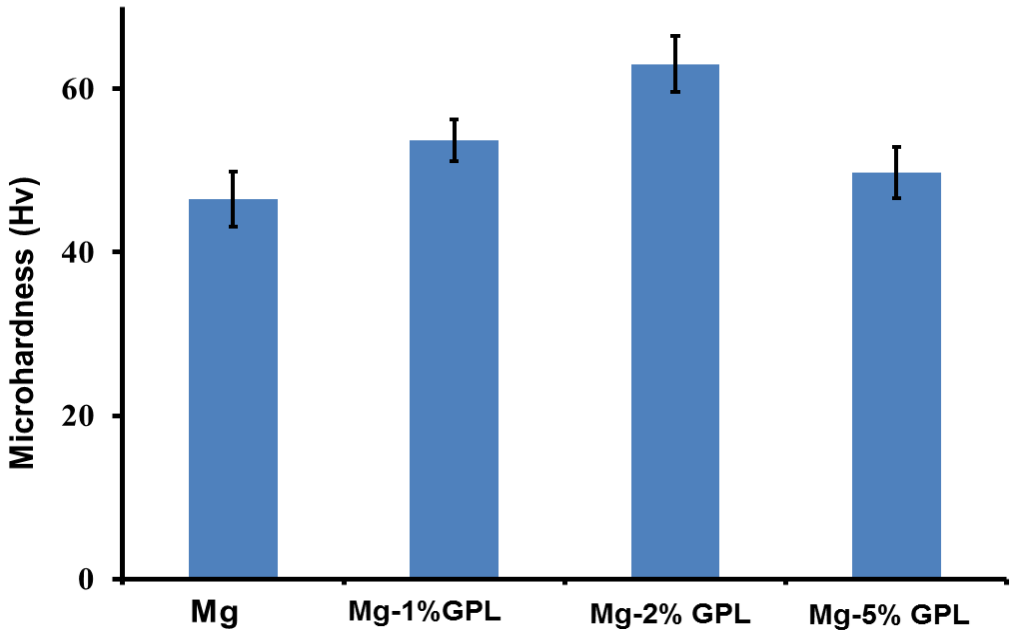

Fig. 3.2 Microhardness data of Mg-GPL composites

Microhardness improvements can be attributed as 1) the uniform dispersion of graphene platelets and little amount of agglomeration of GPL in soft Mg matrix 2) the prevention of localized plastic deformation due to presence of GPL 3) small amount of porosity due to novel processing technique. Dispersion agent, PAA helped to disperse GPL in Mg matrix. In general, graphene nano platelets are wrapped though in situ radial polymerization by PAA [99]. By opening the bonds, free radical initiator of graphene platelets are activated which participates in polymerization. Graphene platelets always contain some defects which also help the graphene platelets to activate easily.

3.1.3.2 Compression testing

Addition of GPL decreased the ultimate compressive strength (UCS) of Mg-GPL composites as shown in Fig. 3.3. The reduction of UCS after addition of graphene platelets can be attributed as the agglomeration of GPLs. Graphene platelets are difficult to disperse in metal matrix due to their large specific surface area and tend to form graphite though van der Waals attraction force. And the agglomeration of GPLs suppressed the strengthening effect of 2-D nano platelets in this experiment.

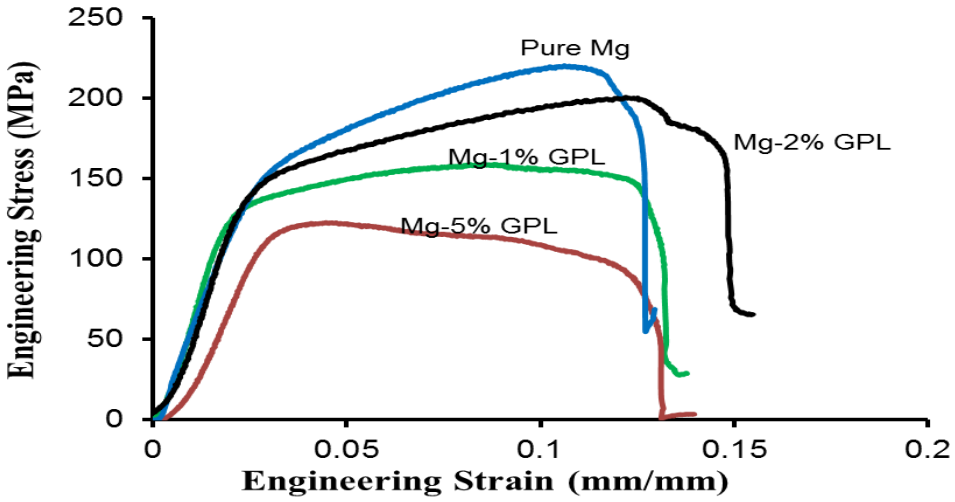

Fig. 3.3 Stress-strain diagram of pure Mg, Mg-1% GPL, Mg-2% GPL, and Mg-5% GPL

From Fig. 3.3, it is also found that the GPL increased the ductility of Mg composites in compression testing. Mg-2% GPL composite shows 9% increment of ductility compared to pure Mg. In case of compressive load, the main deformation mechanism is twinning instead of slip domination [100]. However, slip planes can also contribute in the deformation of materials at compressive load. Usually, Mg has limited ductility at room temperature due to its hexagonal closed packed structure. In room temperature, Mg slips on the base plane (0001) in the <1120> direction and secondary slip on vertical face planes (1010) in the <1120> direction. However presence of reinforcement can generate non-basal slip planes. Improvement of ductility was also

observed in the compression test of Mg-CNT composites [79]. The explanation for the increment of ductility in Mg/CNT composite was the activation of prismatic slip plane by addition of CNTs. In our experiment, the increment of ductility can be predicted as the activation of non-basal slip planes. However, ductility started to decrease when the content of GPL overrun a value of 2 Vol %.

3.1.3.3 Fracture behavior

Macroscopically, Mg and Mg-GPL samples failed primarily due to the formation of one principle crack which was inclined at 45° to the loading axis as seen in Fig. 3.4. Failure initiated near the end of the specimen and all the samples were split into 2 parts. This result suggested that the failure mechanism of pure Mg and Mg-GPL composites were the same under compression. SEM images of fractured surfaces of Mg and Mg-GPL composites revealed the presence of shear bands as seen in Fig. 3.5. The presence of share bands can be attributed as the presence of twinning shear [68, 100]. However, TEM studies are needed to investigate twinning of Mg and Mg-GPL composites and verify the presence of share band.

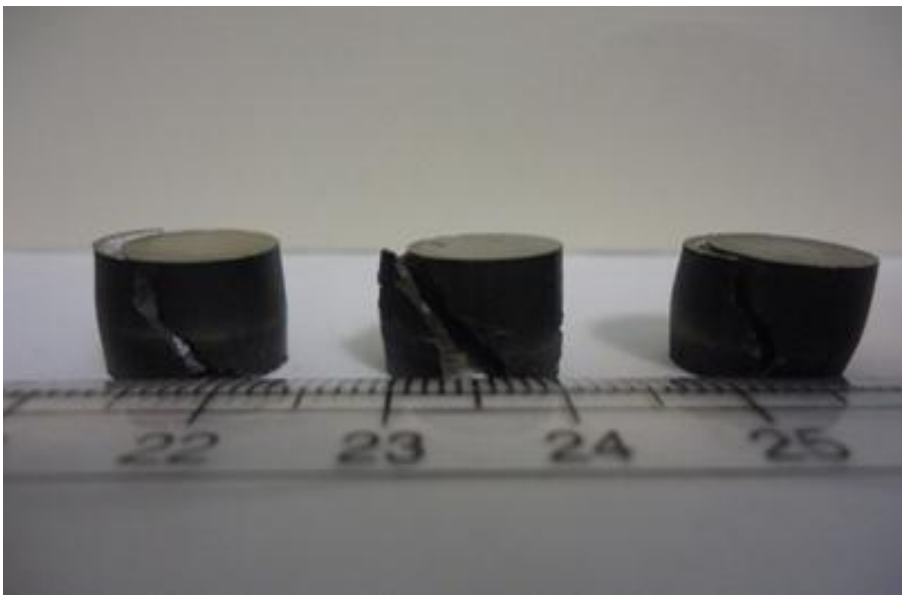

Fig. 3.4 Macrographs of Mg, Mg-2 % GPL, and Mg-5% GPL samples after compressive fracture

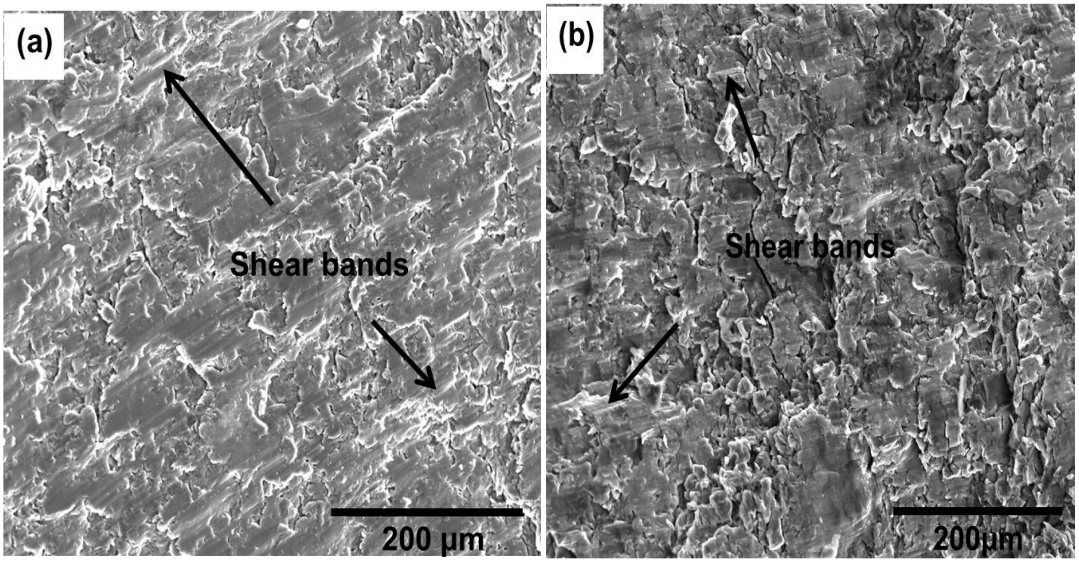

Fig. 3.5 Fractured surfaces of (a) pure Mg, and (b) Mg-2% GPL showing formation of shear bands

Fig. 3.6 shows the high resolution SEM images of fractured surfaces of pure Mg, Mg+2%GPL, Mg+5% GPL composites. Pure Mg shows a micro crack which propagated though the sample and initiated failure. Mg-2% GPL composite shows the presence of micro void due to wider micro cracks than pure Mg. The formation of micro-voids reduced the compressive strength of Mg-2%GPL composites. Mg-5% GPL shows the presence of graphene platelet cluster which further reduced the strength of the Mg-GPL composite.

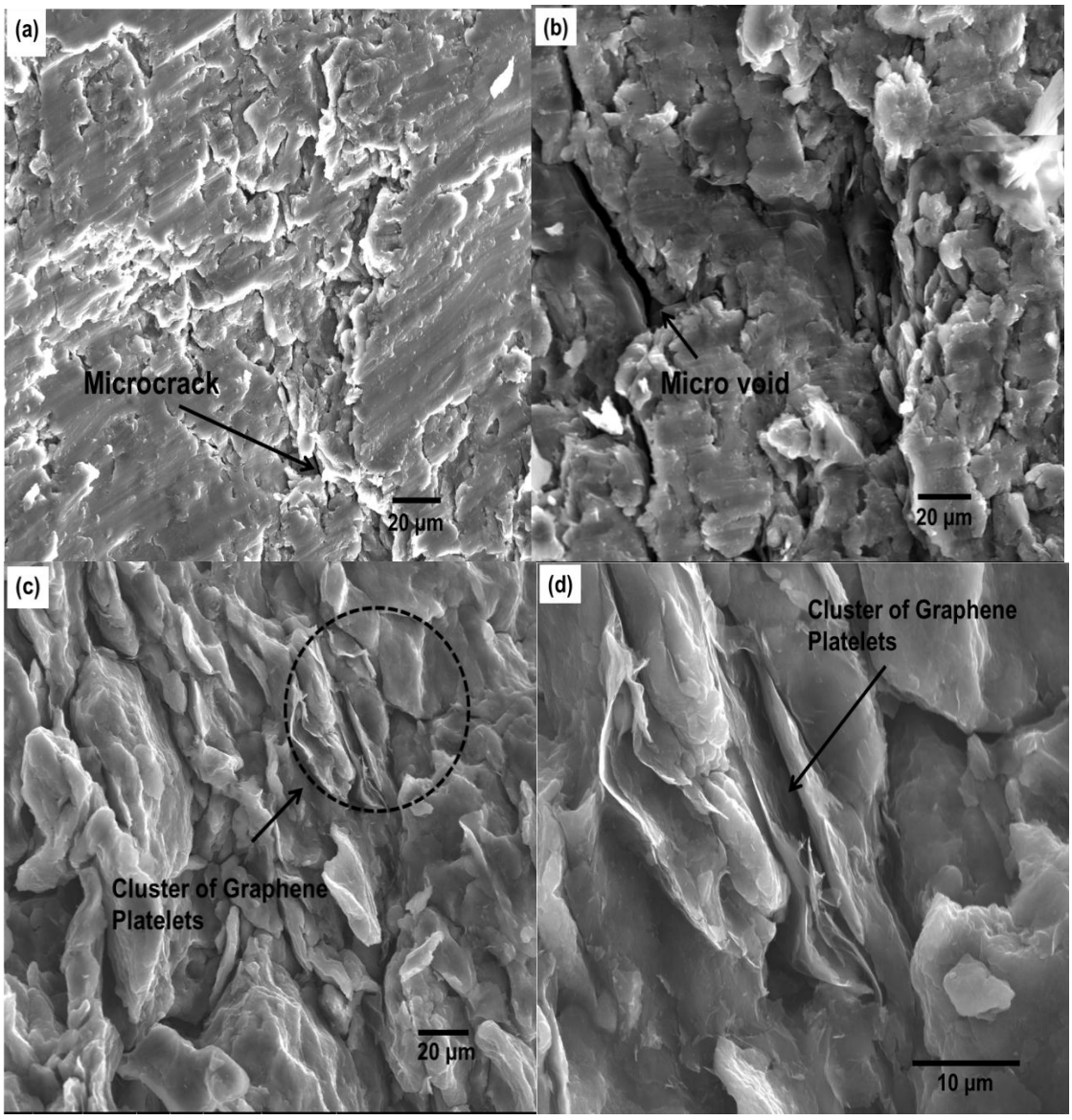

Fig. 3.6 SEM images of fractured surfaces of (a) pure Mg, (b) Mg-2% GPL, (c) Mg-5% GPL, and (d) high magnification image of Mg-5 % GPL

3.1.4 Tribological behavior

Wear loss of pure Mg and Mg-GPL composites against sliding time are plotted in Fig. 3.7. From this graph it can be concluded that the wear loss decreases with the increment of graphene content

in Mg-matrix. Mg-5% GPL shows 34% reduction of weight loss compared to monolithic Mg materials.

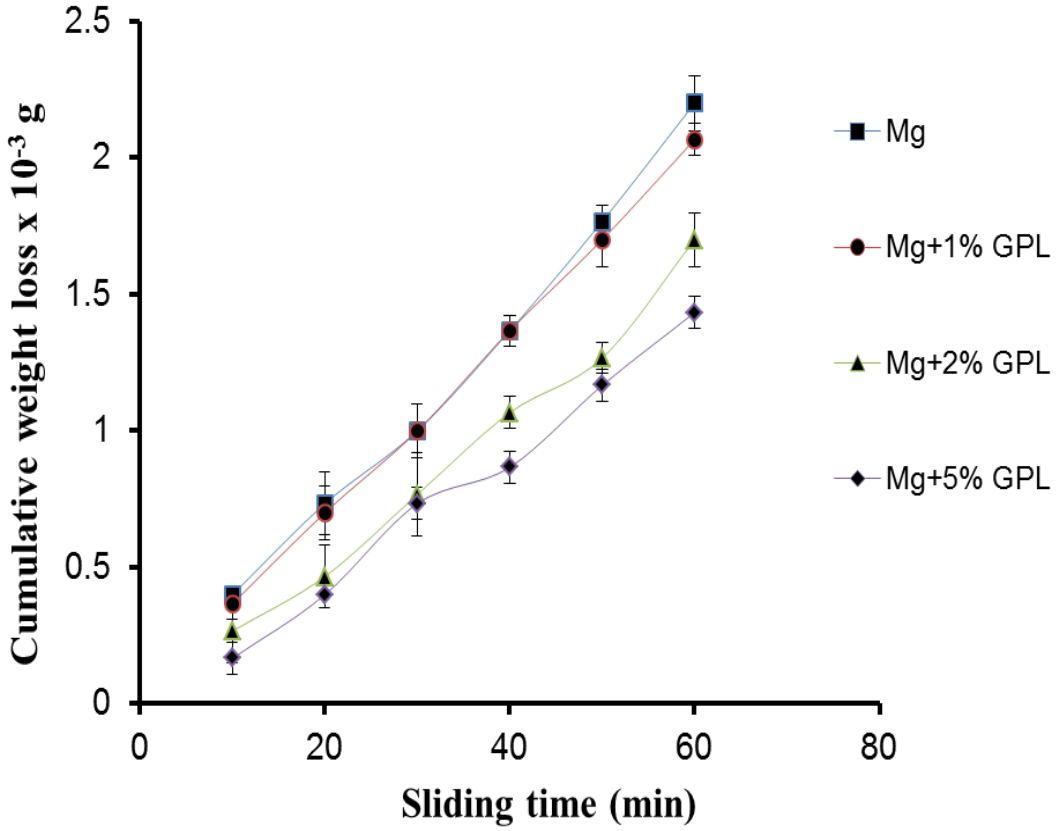

Fig. 3.7 Wear loss as a function of sliding time for pure Mg and Mg-GPL composites

Friction coefficient of pure Mg and Mg-GPL composites are plotted in Fig 3.8. Readings were taken after 10 minutes interval. After 10 minutes of wear testing, samples were cleaned by using acetone and the counter face pin was rotated so that new surface can come in contact for the next reading. In Mg and Mg-5% GPL composites, at the initial stage of each cycle, the friction coefficient was less than 0.1. And in the next stage μ increased tremendously and reached a value more than 1. At the initial stage, the wear mechanism was two body abrasions where contacting materials were magnesium or magnesium composites and counter material was alumina. At the second stage, due to the accumulation of wear debris on the wear track, third body abrasion

started and increased the contact area as well as friction coefficient. Average friction coefficient graph shows that the value μ is unstable in case of pure Mg and it fluctuates in a wide range. After addition of graphene platelets this fluctuations become reduced and the most stable condition was obtained in case of Mg-5% GPL composites. It can be concluded that the tribological behavior will become stable after reinforcement of graphene nano-platelets. This type of phenomena was also observed in case of CNT-Mg_2Si/MgO reinforced Mg composites [101]. Reduction of wear loss indicates the lubricating effect of graphene platelets which is effective to improve the tribological properties of the Mg-matrix composites by decreasing the wear loss and average friction coefficient during sliding.

Fig. 3.9 shows the profilometer reading of pure Mg and Mg-5% GPL composites. After 1 hour of wear testing, Mg sample shows maximum wear depth of 23 μm whereas Mg-5% GPL sample shows a maximum wear depth of 13 μm. Surface profiles show that wear width also reduced after addition of graphene platelets. Pure magnesium also shows more plastic deformation and material pile up compared to Mg-5% GPL composites. These things clearly indicate the improvement of wear properties after addition of graphene platelets.

(a)

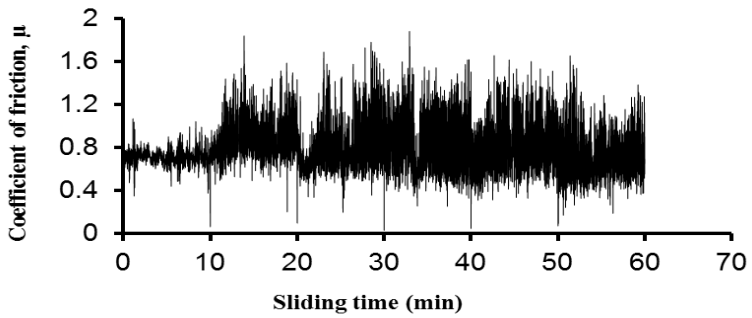

(b)

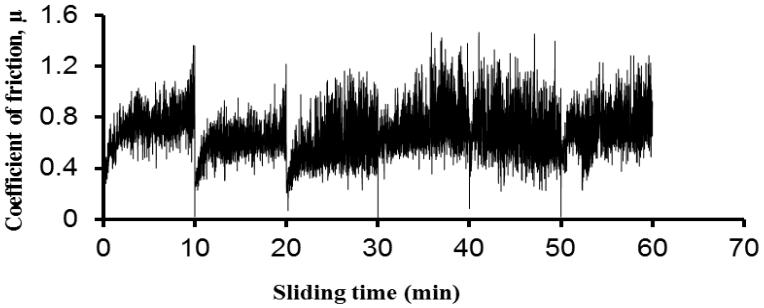

(c)

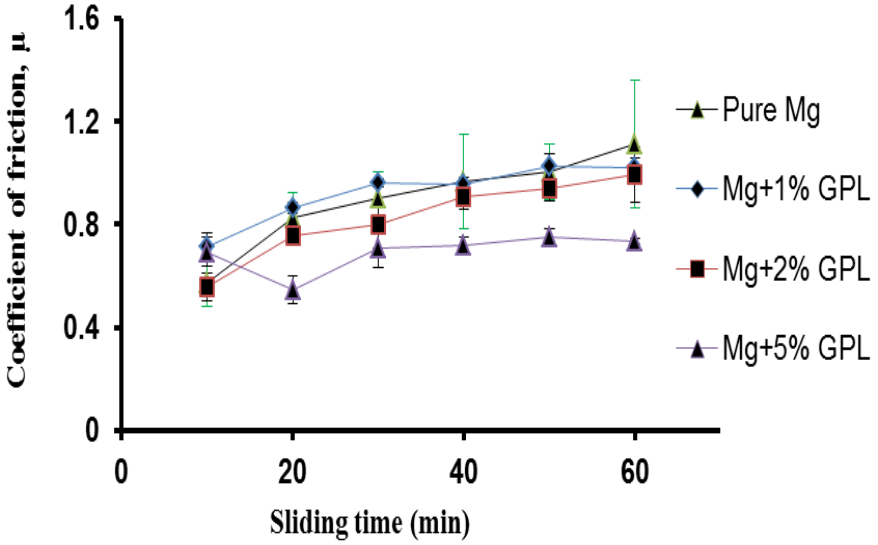

Fig. 3.8 Friction coefficient as a function of sliding time for (a) pure Mg, (b) Mg-5% GPL, and (c) average friction coefficient as a function of sliding time for pure Mg, Mg-1% GPL, Mg-2% GPL, Mg-5% GPL

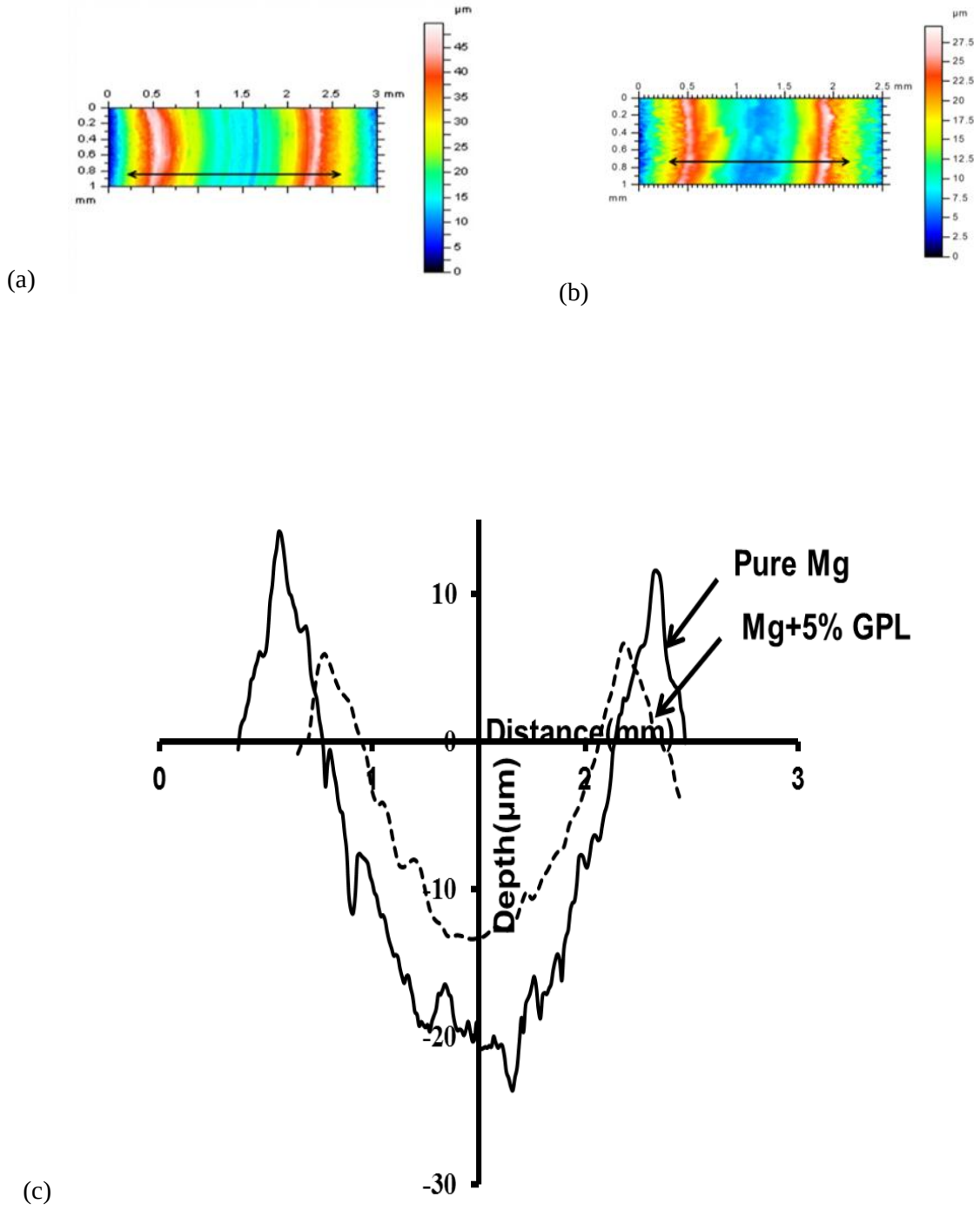

Fig. 3.9 Surface profiles for wear tracks of (a) pure Mg, (b) Mg-5% GPL, and (c) depth profiles across the wear tracks of pure Mg and Mg-5% GPL composites

The scanning electron microscopy (SEM) images of typical worn surfaces of Mg-GPL composites where shown in Fig. 3.10. The wear track of Mg showed a deformed surface and the deformation was along the direction of the motion. All the samples showed grooves parallel to the sliding direction indicates the wear mechanism was abrasion. In abrasion, hard asperities on the alumina counterface plough or cut into the disk and create material removal as small chips. Discernible layers of wear debris on the wear track of magnesium samples indicate the presence of adhesion wear mechanism. However, significance of adhesive wear was less in case of Mg-GPL composites compared to unreinforced Mg samples. After addition of GPL, the surface becomes relatively smoother compared to pure Mg. Due to the presence of small amount of Graphene in Mg-2% GPL composites, no Graphene was observed on the SEM images of wear track. In case of Mg+5% GPL composites, GPL is observed in the wear track and some broken platelets are present in there. Graphene on the surface acts as a lubricant and improves the wear properties of the composites by helping sliding of the counter materials over the surface instead of pressing against the asperities.

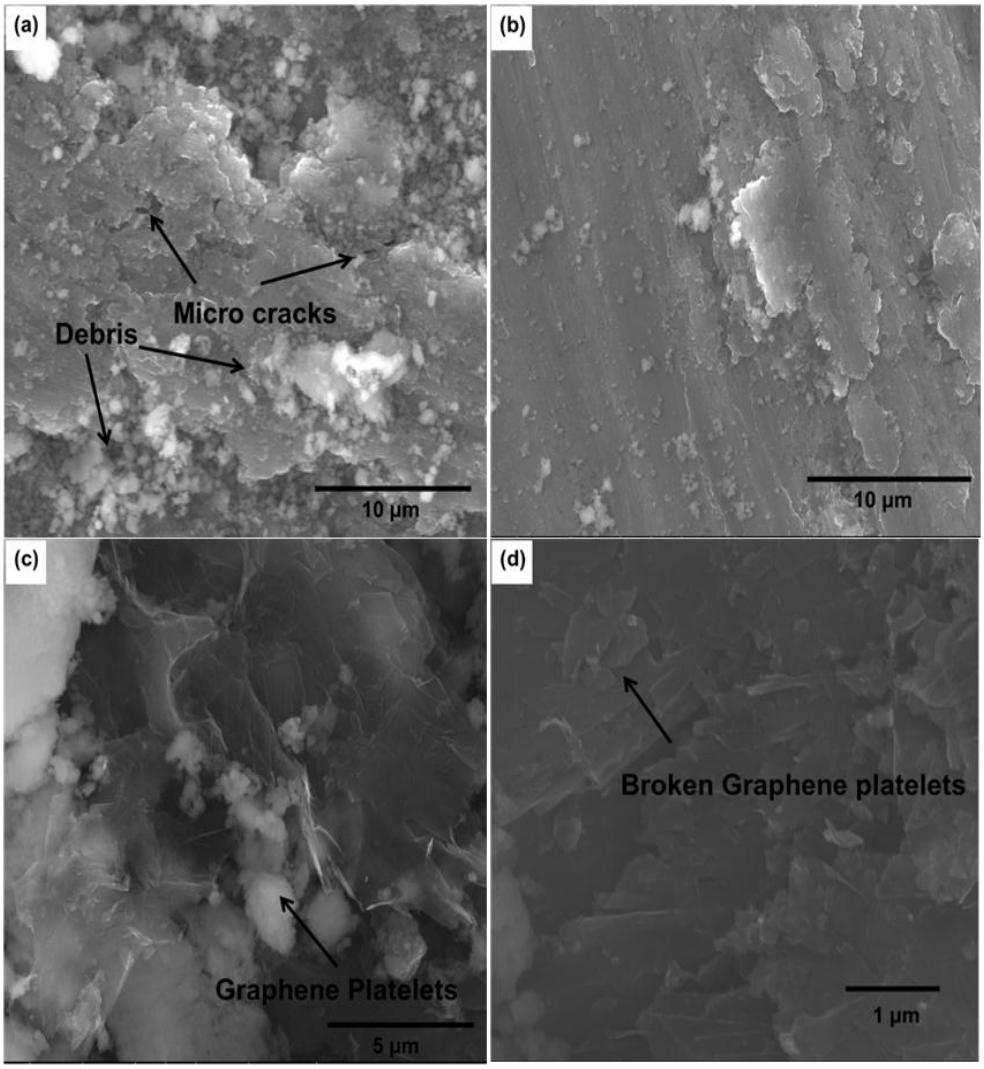

Fig. 3.10 Wear tracks of SPS sintered (a) pure Mg, (b) Mg-2% GPL, (c) Mg-5 % GPL, and (d) high magnification image of Mg-5% GPL showing broken graphene platelets on wear track

3.2 Spark plasma sintering of nano-SiC reinforced Mg matrix composites

3.2.1 Density

Table 3.2 shows the density of pure Mg and Mg-nano SiC composites. From the density data it is found that using the same sintering parameters, the density of Mg-nano SiC increased. It is also seen from the table that nearly full densification was attained (≈ 98%) in case of pure magnesium sintered at a temperature of 450° C and a pressure of 50 MPa. However full densification (relative density > 99%) was observed in case of Mg-1% nano SiC, and Mg-2% nano SiC composites. Full densification can be attributed to the presence of SiC nanoparticles which increases surface diffusion due to their high surface area. In case of Mg-4% nano SiC composites, the reduction of density value can be attributed to the crack growth near the agglomerated silicon carbide regions. Formation of crack creates void and debonding starts the particle-matrix interfaces.

Table 3.2 Density of Mg-nano SiC composites

Composition	Theoretical density (g/cm^3)	Experimental density (g/cm^3)	Relative Density (%)
Mg	1.74	1.70	97.58
Mg-1% nano SiC	1.75	1.75	99.84
Mg-2% nano SiC	1.77	1.76	99.28
Mg-4 %nano SiC	1.80	1.76	97.88

3.2.2 X-ray diffraction analysis

The X-ray diffraction pattern from the spark plasma sintered pure Mg and Mg-nano SiC samples are presented in Fig 3.11. Characteristic peak corresponding to SiC could not be found in the XRD pattern from the Mg- 2 % nano SiC composites. This could be due to low volume fraction of SiC nanoparticles. In case of Mg-4% nano-SiC sample, SiC peaks were observed. Reaction products such as MgO and Mg_2Si were not observed in at the Mg and SiC interface which was observed in case Mg-SiC composites prepared by molten methods [102].

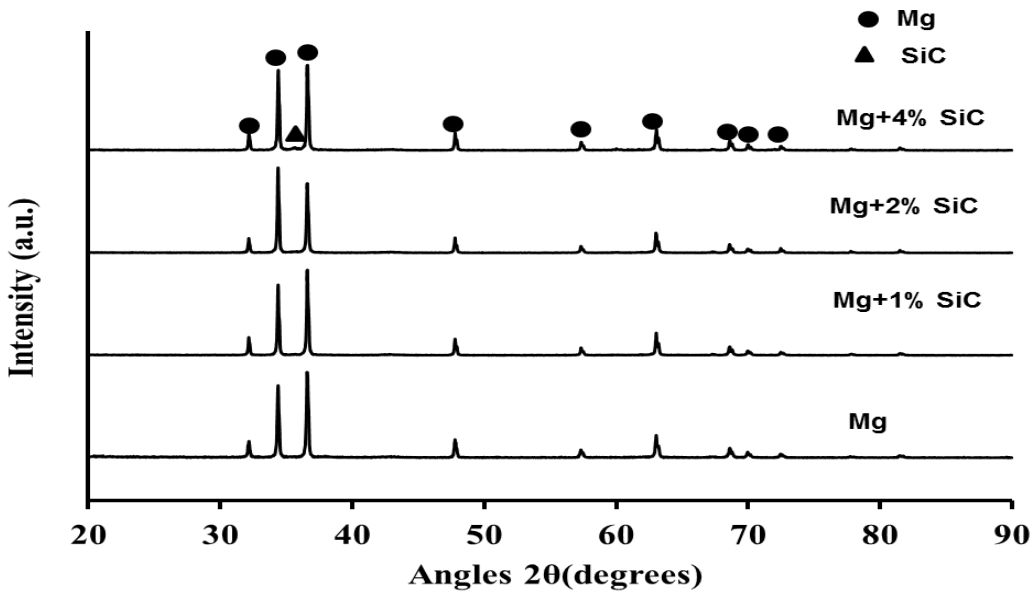

Fig. 3.11 X-ray diffraction patterns from SPS sintered Mg and Mg-nano SiC composites

3.2.3 Mechanical properties characterization

3.2.3.1 Microhardness testing

The average microhardness of Mg-SiC composites with 1, 2, and 4 Vol. % of SiC reinforcement were found to be 70, 76, and 74 HV, respectively (shown in Fig. 3.12). Using the same sintering parameters, the microhardness value of pure Mg was 46 HV. Microhardness values of Mg-nano SiC composites increased significantly compared to unreinforced Mg materials. Microhardness data of Mg- nano SiC composites shows an increasing trend of hardness up to Mg-2 % nano SiC composite. Mg-2% nano SiC shows an increment of 65%. The micro-hardness value of silicon carbide nano-powder is 2840~3240 HV. This higher hardness value of nano-SiC can provided their inherent properties to the soft Mg-matrix and can act as a hindrance to the dislocation motions which attributes towards the improvement of hardness value. Reduction of porosity was another reason behind the improvement of hardness.

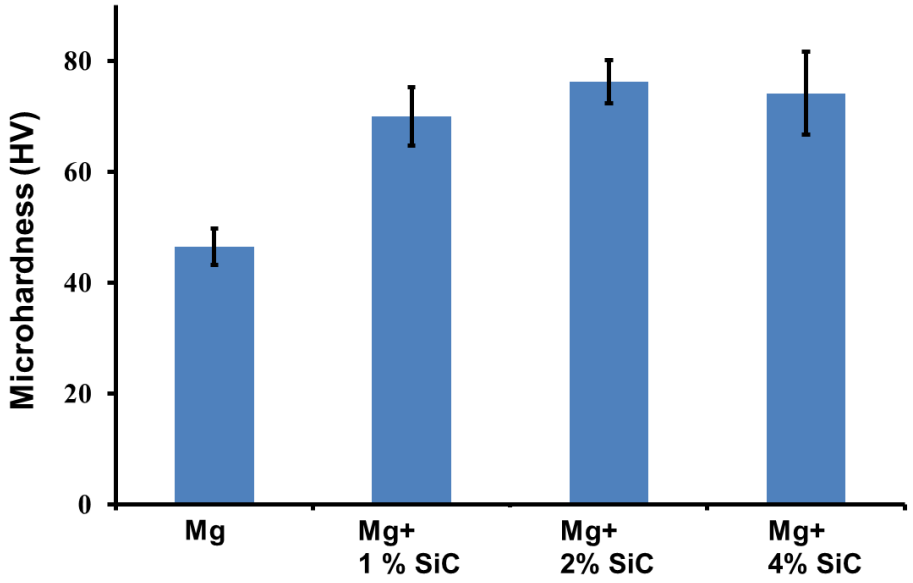

Fig. 3.12 Microhardness data of Mg-nano SiC composites

3.2.3.2 Compression testing

Fig. 3.13 shows the representative compressive stress-strain curve of Mg and Mg-nano SiC composites. From the graph, it is found that addition of 2% nano-SiC particles in Mg-matrix increase the ultimate compressive strength and yield strength significantly. Mg- 2% nano SiC shows 17% improvement of yield strength and 12 % improvement of UCS. Significant improvement of UCS can be attributed as 1) limited agglomeration at the time ball milling which acts as a stress concentration sites 2) development of multi-directional thermal stresses at the Mg/SiC interfaces due to the large difference of co-efficient of thermal expansion between Mg and SiC particles [103, 104] 3) generation of dislocations due to elastic modulus mismatch between the magnesium matrix and nano SiC reinforcements. 103] 4) effective transfer of load from soft matrix to hard particles due to good interfacial bonding [103] and 5) low degree of porosity. Yield stress can be expressed by the dislocation density and magnitude of all the obstacles that restrict the dislocation motion. When load is applied, dislocation moves and this dislocation movement are obstructed by the presence of reinforcing particles and dislocation pile-

ups. Again, multidirectional thermal stress induced during processing starts multi-gliding system and as a result, dislocations start to generate and move in different directions. Finally, these dislocations also agglomerate and forms grain boundary ledges. With the increment of applied load, these ledges also act as a barrier of dislocation motions and as a consequence pile-ups increases. Combined effects of these dislocation pile ups create improvement in yield strength. The increment in yield strength due to thermal mismatch and elastic modulus mismatch can be calculated by using following equation [105]

$$\Delta\sigma = \sqrt{(\llbracket\Delta\sigma_{EM})\rrbracket^2 + (\Delta\sigma_{CTE})^2} \ldots\ldots\ldots\ldots\ldots\ldots\ldots\ldots\ldots\ldots\ldots\ldots\ldots\ldots\ldots\ldots\ldots\ldots\ldots \mathbf{(5)}$$

Where, $\Delta\sigma_{EM}$ and $\Delta\sigma_{CTE}$ are the increment of stress due to elastic modulus and co-efficient of thermal energy mismatch. However, further increase in nano-SiC particles content from 2 Vol% to 4 Vol% lead to reduction in ultimate compressive strength of the composite. With the increment of nano-SiC contents, debonding starts at matrix-reinforcement interfaces due to agglomeration of nano-SiC particles which acts as a stress concentrator. In case of Mg-4% SiC, the effect of clusters of nano-SiC particles is higher than the combined effects of thermal stress and partial dispersion of the nanoparticles. As a result ultimate compressive strength decreased as the volume fraction of SiC reaches to 4%.

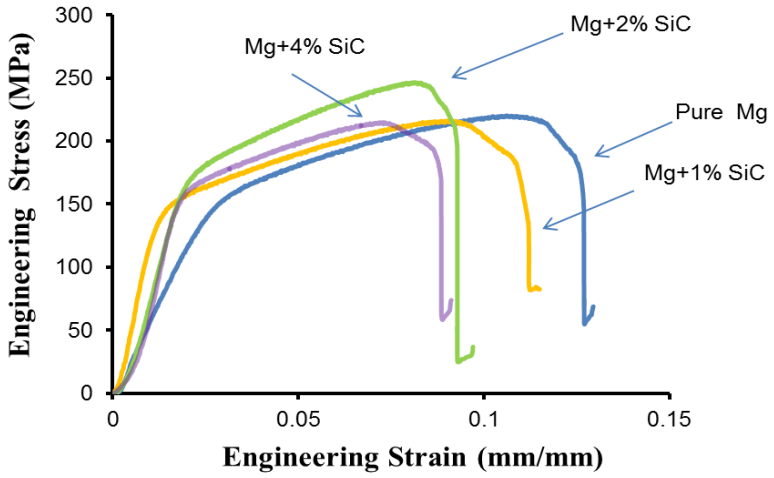

Fig. 3.13 Compression testing data of Mg-nano SiC composites

3.2.3.3 Fracture behavior

In case of Mg-nano SiC samples, failure initiated near the end of the specimen due to formation of one principle crack at maximum load which propagates through 45° angle as seen in Fig 3.14. All of the samples were split into 2 parts like Mg-GPL composites and fractured surfaces were inclined to 45° with loading axis.

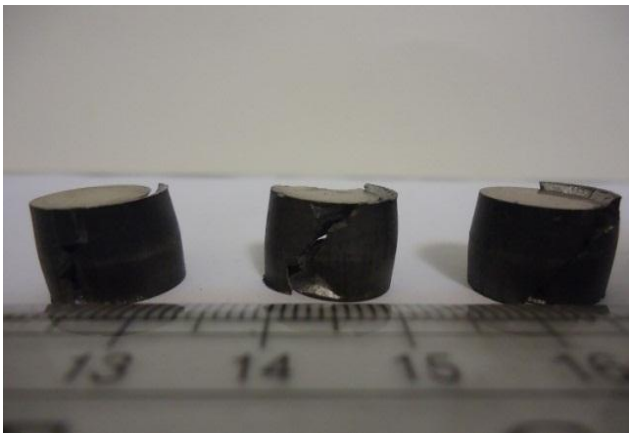

Fig. 3.14 Macrographs of Mg, Mg-2% nano SiC, and Mg-4% nano SiC samples after compressive fracture

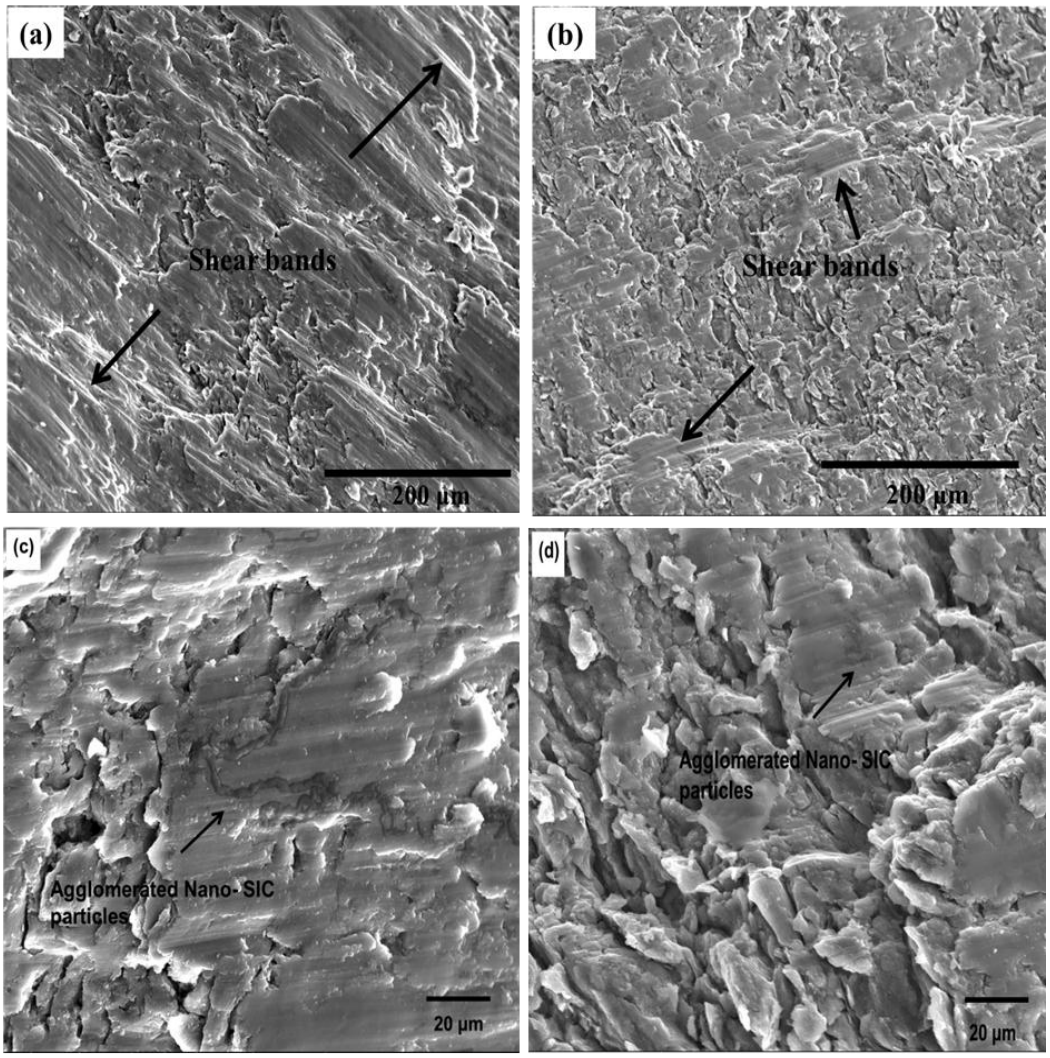

Fig. 3.15 Fractured surfaces of (a) Mg-2% nano SiC, (b) Mg-4% nano SiC showing shear bands, (c) high magnification SEM images of Mg-2% nano SiC, and (d) Mg-4% nano SiC

SEM images of fractured surfaces of Mg- 2% nano SiC and Mg-4% nano SiC composites are shown in Fig. 3.15. Formation of shear band was observed from low resolution images of fractured surfaces of the composites which indicate ductile failure of the composites. High resolution images of Mg-2% nano SiC and Mg-4% nano SiC show agglomerated SiC nano

particles on the surface. These agglomerates reduced the strengthening effect of hard SiC particles.

3.2.3.3 Tribological behavior

Fig.3.16 shows cumulative weight loss as a function of sliding time for pure Mg, Mg+1% nano-SiC, Mg+2% nano SiC and Mg+4% nano-SiC composites. From the graph it is evident that with the increment of nano SiC contents, the weight loss reduced significantly. Nano SiC whose hardness (2840~3240 HV) is significantly higher than pure Mg (46 HV), acts as an obstacle against wear by resisting plastic flow. Wear loss and depth of wear track shows significant reduction of wear loss after addition of hard particles following Archard equation. The weight loss reduction can also be attributed to the ability to maintain a stable and thick oxide film by the presence of SiC particles and as a result Mg-SiC composites show better load bearing capacity [106]. However, Mg+4 % SiC shows higher weight loss compared to unreinforced Mg. This higher wear loss can be attributed to pull out and machining away of SiC particles from the Mg matrix and formation of delamination wear of Mg-4% nano SiC composite due to excessive reinforcement. Delamination wear initiated from the subsurface cracks formation at the particle matrix interface due to agglomeration. This type of phenomenon was observed in case of Al_2O_3 and SiCp reinforced Mg-matrix composites at low loads [107,108]. Fig. 3.17 shows friction coefficient as a function of sliding time. From this graph, it is found that coefficient of friction significantly decreases after addition of SiC nanoparticles. However, the friction coefficient become almost constant when the reinforcement content reaches to 4 Vol%.

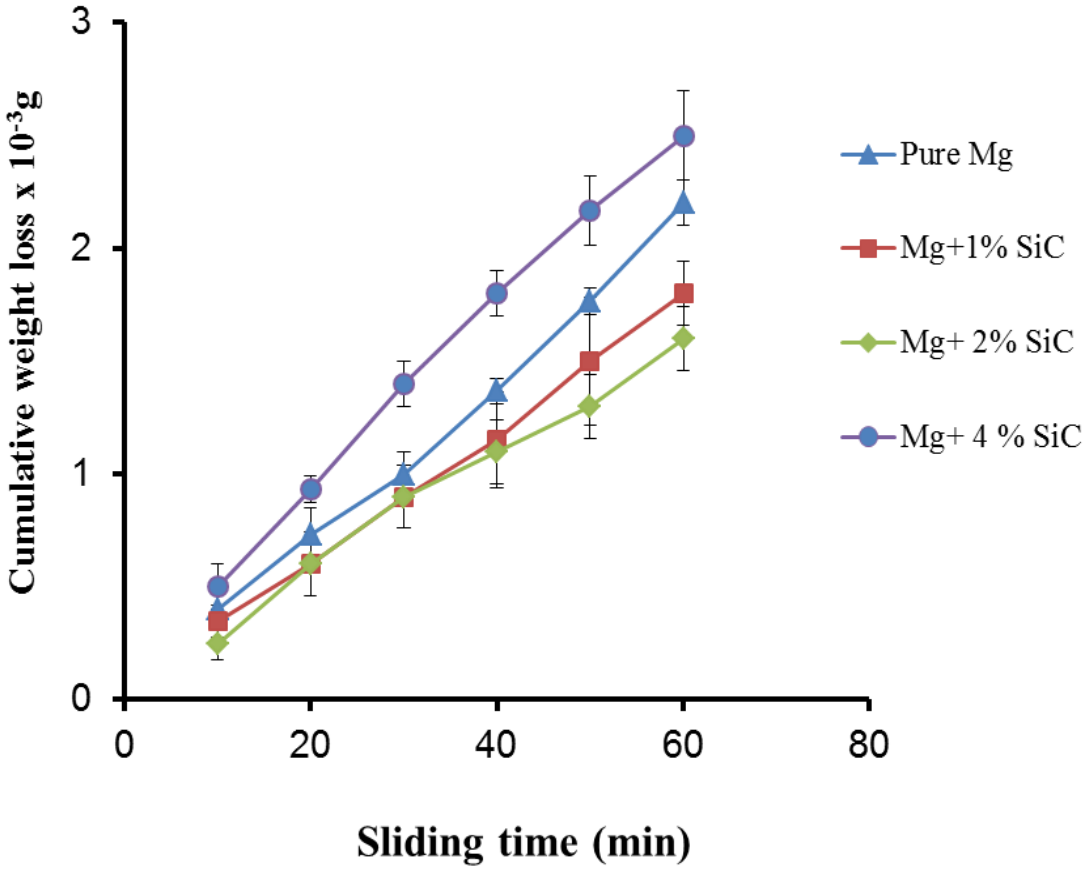

Fig. 3.16 Cumulative weight loss as a function of sliding time for different Mg-nano SiC composites

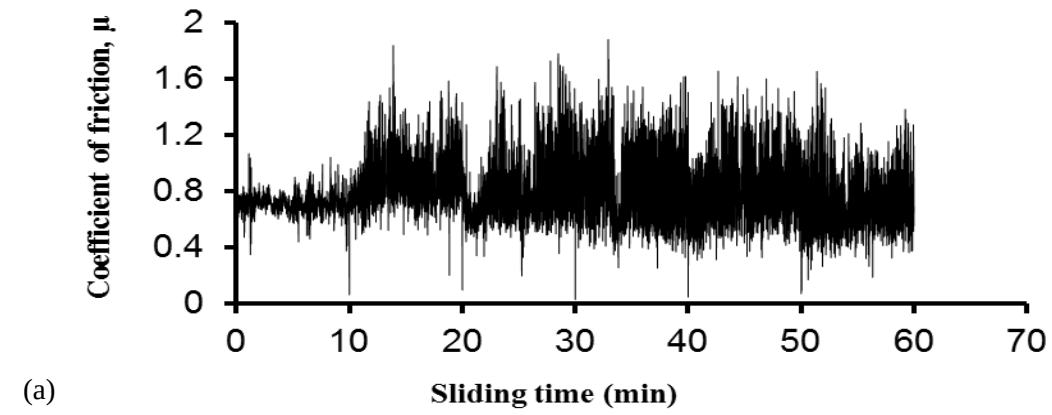

(a)

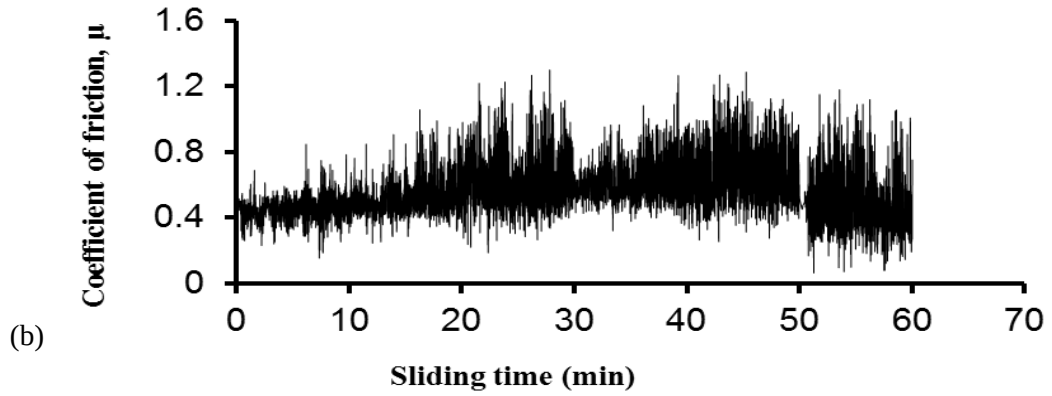

(b)

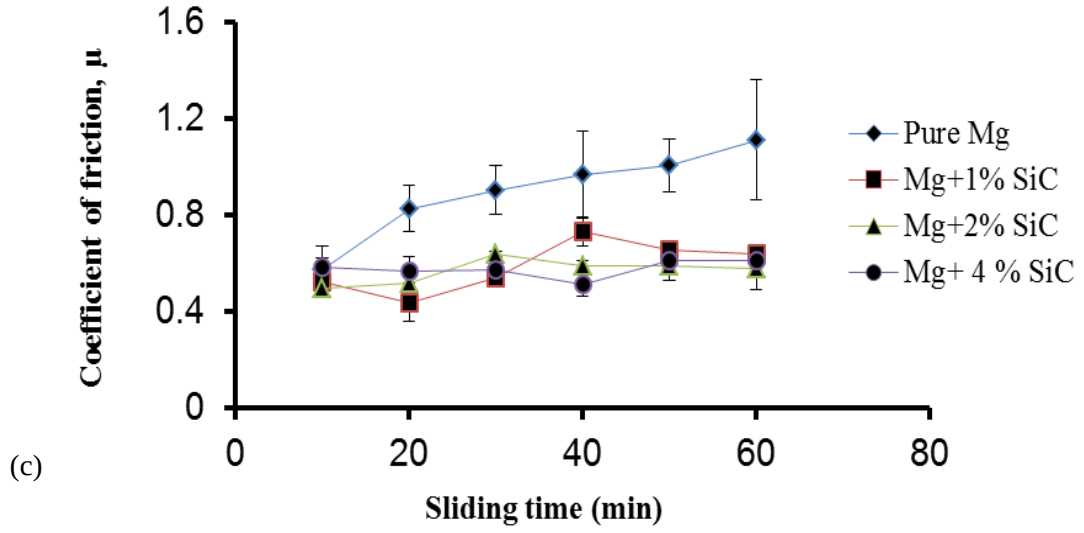

(c)

Fig. 3.17 Friction coefficient as a function of sliding time for (a) pure Mg, (b) Mg-2% nano SiC, and (c) average friction coefficient as a function of sliding time for Mg-nano SiC composites having different SiC contents

Profilometer reading of pure Mg and Mg-2% nano SiC composites are shown in Fig. 3.18. After 1 hour of wear testing, Mg -2% nano SiC shows significant reduction in wear depth compared to unreinforced Mg samples. Surface profiles show that wear width also reduced after addition of nano-SiC particles. However, the Profilometer reading of Mg-2% nano- SiC shows an irregular wear track which may be attributed to the presence of hard nano-SiC particles in the wear track or SiC agglomerates.

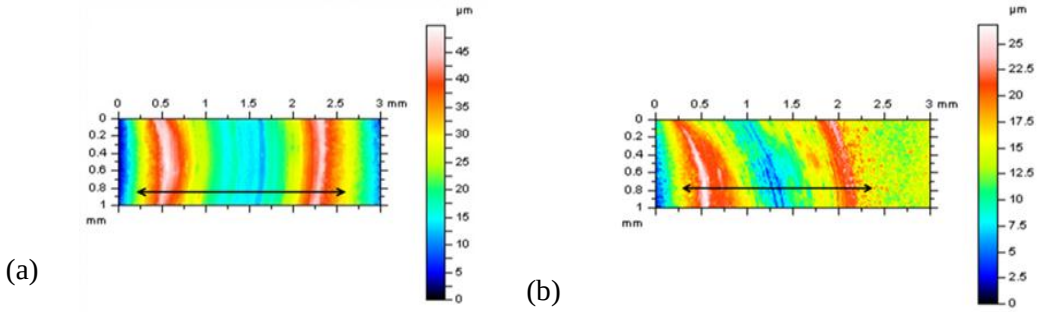

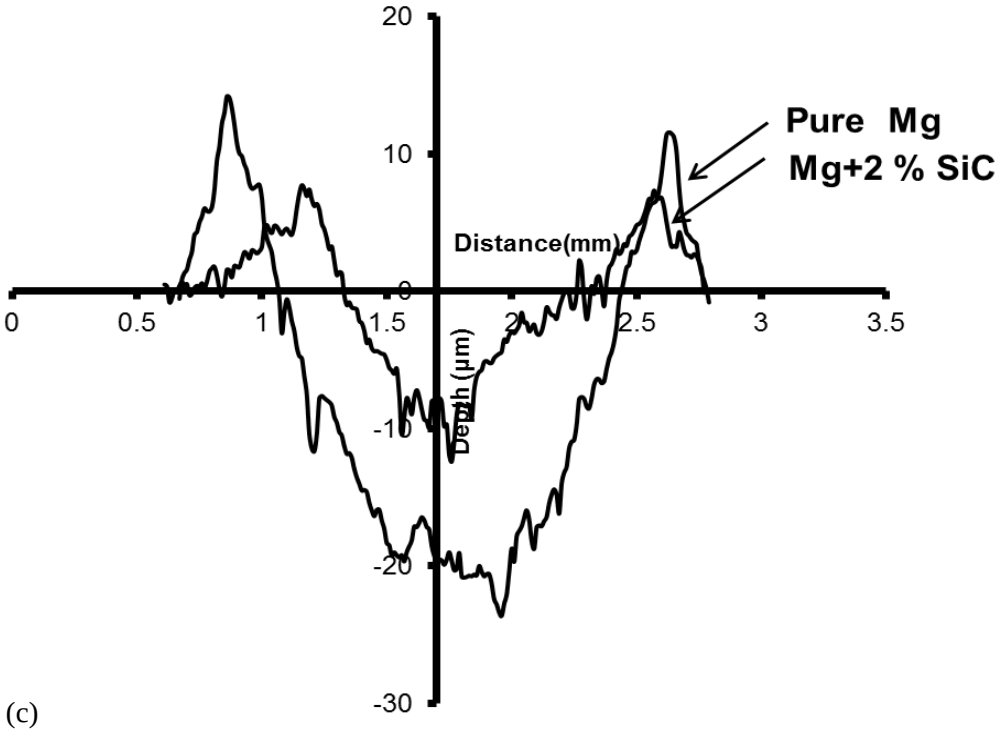

Fig.3.18 Surface profiles for wear tracks of (a) pure Mg, (b) Mg-2% nano SiC, and (c) depth profiles across the wear tracks of Mg and Mg-nano SiC

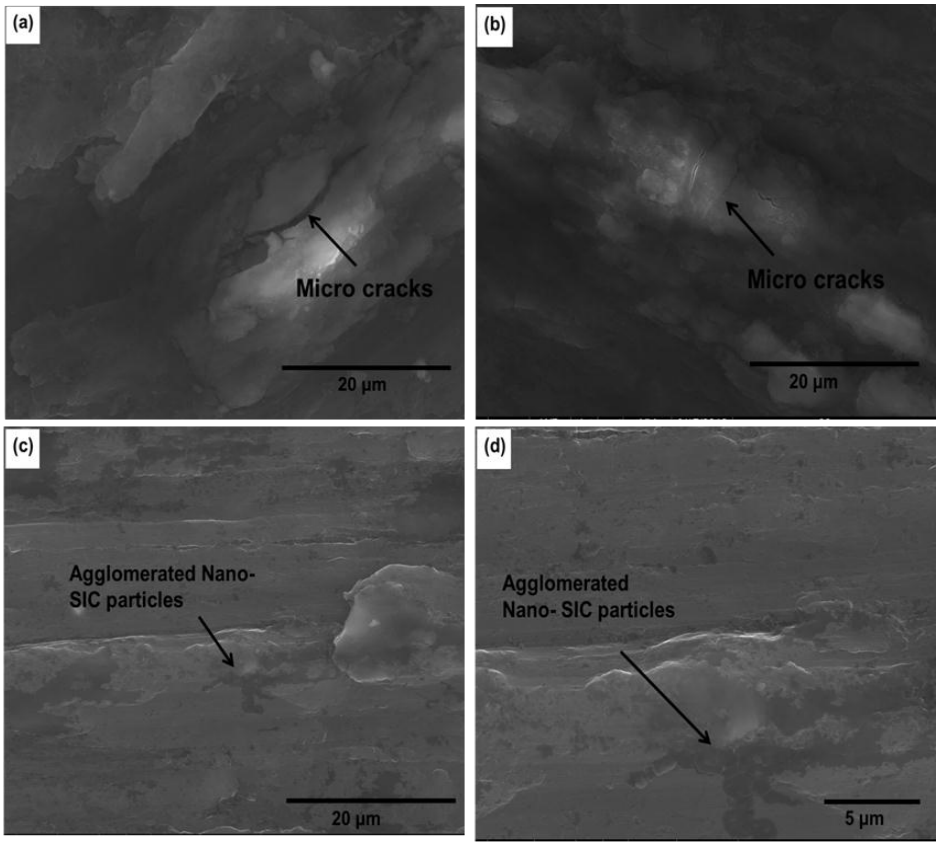

Fig. 3.19 Wear tracks of SPS sintered (a) pure Mg, (b) Mg-2% nano SiC, (c) Mg-4% nano SiC, and (d) high magnification image of Mg-4% nano SiC showing agglomerated SiC particles on wear track

The SEM images of wear tracks of Mg-nano SiC composites were shown in Fig. 3.19. Pure Mg, Mg-2% SiC and Mg-4% SiC samples were tested for 1 hour under a normal load of 1 N. The wear track of Mg shows micro-crack along the direction of the track which is wider than those cracks in Mg-2% nano SiC composites. Due to the presence of small amount of SiC in Mg-2% SiC composites, no SiC is observed on the SEM images of wear track. The wear track of Mg-4% nano SiC shows agglomerated SiC particles in the wear track. This agglomerated SiC particles creates weak bonding between Mg and SiC particles and as a result delamination wear occurs and the wear loss was even more than that of pure Mg sample.

CHAPTER IV

CONCLUSIONS

- Spark Plasma sintering technique was used to synthesize pure Mg, Mg-GPL and Mg-nano SiC composites. Applying a sintering temperature of 450° C and pressure 50 MPa, nearly full densification was achieved.
- Graphene platelets of 1 Vol. %, 2 Vol. %, and 5 Vol. % were reinforced in the Mg matrix using spark plasma sintering technique.
- Mechanical characterization revealed that the presence of GPL significantly improved the hardness of the Mg-matrix composites and reached a maximum of 37 % improvement in case of Mg-2% GPL composite. The presence of GPL decreased the yield strength and ultimate compressive strength. Ductility of the composites increased with the increment of GPL contents up to 2 Vol% of GPL. Mg-2 % GPL composites showed 8.7% improvement of the ductility.
- Graphene platelets increased the wear resistance of Mg materials. Improvement of wear resistance can be attributed as the presence of graphene platelets which acted as a lubricant and reduced the contact between hard asperities of counter materials and composites.
- Nano SiC powders of 1 Vol.%, 2 Vol.%, and 4 Vol.% were reinforced in the Mg matrix using spark plasma sintering
- Mg-nano SiC showed significant improvement of hardness, yield strength, ultimate compressive strength and reached maximum in case of Mg-2% nano SiC composite.

Mg-2% nano SiC showed an increment of 18% of yield strength and 12% of ultimate compressive strength. However, ductility was drastically reduced.

- SiC nanoparticles increased the wear resistance of Mg materials. Wear resistance of Mg-nano SiC was increased due to the presence of hard SiC nano particles which acted as a barrier of plastic flow. However, weight loss increased when nano SiC contents overrun to 4 Vol. %. The higher wear loss can be attributed as the delamination between Mg and nano-SiC particles.

CHAPTER V

FUTURE WORKS

- To analyze thermal expansion coefficient of Mg-matrix composites
- To investigate the interfacial chemistry between Mg and GPL by using Transmission Electron Microscopy (TEM)
- To perform nano-indentation test of Mg-GPL and Mg-nano SiC composites
- To analyze the effect of ball milling and sintering over Graphene by using Raman Spectroscopy
- To study compressive behavior of Mg-matrix composites at high temperature

REFERENCES

1. Singh, A., and Harimkar, S. P. (2012). Laser Surface Engineering of Magnesium Alloys: A Review. JOM Journal of the Minerals, Metals and Materials Society, 1-18.

2. Jain, C. C., and Koo, C. H. (2007). Creep and corrosion properties of the extruded magnesium alloy containing rare earth. Materials transactions, 8(2), 265-272.

3. Huang, W., Hou, B., Pang, Y., and Zhou, Z. (2006). Fretting wear behavior of AZ91D and AM60B magnesium alloys. Wear, 260(11), 1173-1178.

4. An, J., Li, R. G., Lu, Y., Chen, C. M., Xu, Y., Chen, X., and Wang, L. M. (2008). Dry sliding wear behavior of magnesium alloys. Wear, 265(1), 97-104.

5. Aung, N. N., Zhou, W., and Lim, L. E. (2008). Wear behaviour of AZ91D alloy at low sliding speeds. Wear, 265(5), 780-786.

6. Kulekci, M. K. (2008). Magnesium and its alloys applications in automotive industry. The International Journal of Advanced Manufacturing Technology, 39(9), 851-865.

7. Shamekh, M. (2011). Processing and Characterization of Mg Matrix Composites Reinforced with TiC and TiB2 Phases using an In-situ Reactive Infiltration Technique (Doctoral dissertation, Concordia University)

8. Kainer, K. U. (1991). Influence of the production technique and type of reinforcement on the properties of magnesium-matrix-composites. Composite Material Technology-1991 (Vol. 1, pp. 191-197).

9. Leon-Patino, C. A. (2001). Infiltration processing of metal matrix composites using coated ceramic particulates.

10. Lloyd, D. J. (1994). Particle reinforced aluminium and magnesium matrix composites. International Materials Reviews, 39(1), 1-23.

11. Zheng, M., Wu, K., Liang, H., Kamado, S., and Kojima, Y. (2002). Microstructure and mechanical properties of aluminum borate whisker-reinforced magnesium matrix composites. Materials Letters, 57(3), 558-564.

12. Sukumaran, K., Ravikumar, K. K., Pillai, S. G. K., Rajan, T. P. D., Ravi, M., Pillai, R. M., and Pai, B. C. (2008). Studies on squeeze casting of Al 2124 alloy and 2124-10% SiCp metal matrix composite. Materials Science and Engineering: A, 490(1), 235-241.

13. Kainer, K. U. (Ed.). (2003). Magnesium alloys and technology (pp. 1-23). Wiley-VCH.

14. Spencer, D. B., Mehrabian, R., and Flemings, M. C. (1972). Rheological behavior of Sn-15 pct Pb in the crystallization range. Metallurgical and Materials Transactions B, 3(7), 1925-1932.

15. Lee, D. M., Suh, B. K., Kim, B. G., Lee, J. S., and Lee, C. H. (1997). Fabrication, microstructures, and tensile properties of magnesium alloy AZ91/SiC p composites produced by powder metallurgy. Materials science and technology, 13(7), 590-595.

16. Mehrabian, R., Riek, R. G., and Flemings, M. (1974). Preparation and casting of metal-particulate non-metal composites. Metallurgical and Materials Transactions B, 5(8), 1899-1905.

17. Hollinggrak, J. (1819). Casting of metals. UK Patent, (4371).

18. Tsherhoff, D. K. (1880). On the Structure of Cast-Steel Ingots. Proc. Institute of Mechanical Engineers, 152.

19. V. G. WELTER, Z. Metallkd. 23 (1931) 255

20. Wu, K., Zheng, M., Yao, C., Sato, T., Tezuka, H., Kamio, A., and Li, D. X. (1999). Crystallographic orientation relationship between SiCw and Mg in squeeze-cast SiCw/Mg composites. Journal of materials science letters, 18(16), 1301-1303.

21. Wu, K., Zheng, M., Zhao, M., Yao, C., and Li, J. (1996). Interfacial reaction in squeeze cast SiCw/AZ91 magnesium alloy composite. Scripta materialia, 35(4).

22. Zheng, M., Wu, K., Liang, H., Kamado, S., and Kojima, Y. (2002). Microstructure and mechanical properties of aluminum borate whisker-reinforced magnesium matrix composites. Materials Letters, 57(3), 558-564.

23. Luo, A., Renaud, J., Nakatsugawa, I., and Plourde, J. (1995). Magnesium castings for automotive applications. Journal of the Minerals, Metals and Materials Society, 47(7), 28-31.

24. Hashim, J., Looney, L., and Hashmi, M. S. J. (1999). Metal matrix composites: production by the stir casting method. Journal of Materials Processing Technology, 92, 1-7.

25. Luo, A. (1995). Processing, microstructure, and mechanical behavior of cast magnesium metal matrix composites. Metallurgical and Materials Transactions A, 26(9), 2445-2455.

26. Saravanan, R. A., and Surappa, M. K. (2000). Fabrication and characterisation of pure magnesium-30 vol.% SiC P particle composite. Materials Science and Engineering: A, 276(1), 108-116.

27. Gui, M., Li, P., and Han, J. (2003). Fabrication and characterization of cast magnesium matrix composites by vacuum stir casting process. Journal of materials engineering and performance, 12(2), 128-134.

28. Mikucki, B. A., Mercer, W. E., and Green, W. G. (1990). Extruded magnesium alloys reinforced with ceramic particles. Society of Automotive Engineers.

29. Lim, S. W., and Choh, T. (1992). Mechanical Properties of SiC Particulate Reinforced Magnesium Matrix Composites Fabricated by Melt Stirring Method. Journal of the Japan Institute of Metals(Japan), 56(9), 1101-1107.

30. Holden, P. E., Pilkington, R., Lorimer, G. W., King, J. F., and Wilks, T. E. (1996, April). The tensile and creep behavior of a Mg-alloy matrix SiC reinforced composite. In Proceedings of the Third International Magnesium Conference (pp. 647-662).

31. Singer, A. R. (1985). U.S. Patent No. 4,515,864. Washington, DC: U.S. Patent and Trademark Office.

32. Clyne, T. W. (2001). Metal matrix composites: Matrices and processing. Elsevier, 1-14.

33. Ebert, T., Moll, F., and Kainer, K. U. (1997). Spray forming of magnesium alloys and composites. Powder metallurgy, 40(2), 126-130.

34. Kainer, K. U., and Moll, F. (1996). Microstructure and properties of magnesium-SiCp-composites influenced by production techniques and particle shapes. Automotive Automation Limited(England),, 363-369.

35. Noguchi, A., Ezawa, I., Kaneko, J., and Sugamata, M. (1995). SiCp/Mg-Ce and Mg-Ca alloy composites obtained by spray forming. Japan Institute of Light Metals, Journal, 45(2), 64-69.

36. Tham, L. M., Gupta, M., and Cheng, L. (1999). Influence of processing parameters on the near-net shape synthesis of aluminium-based metal matrix composites. Journal of Materials Processing Technology, 89, 128-134.

37. Idris, J., Tan, J. C., and Chang, C. W. (2001). The Development of Advanced Materials-High Performance Properties of Composite for Automotive and Aerospace Applications. Journal of Science & Technology, 9(2), 149-158.

38. Rudaajevová, A., and Lukáč, P. (1999). Thermal Properties of Reinforced QE22 Magnesium Alloy. physica status solidi (a), 175(2), 457-465.

39. Badini, C., Marino, F., Montorsi, M., and Guo, X. B. (1992). Precipitation phenomena in B4C-reinforced magnesium-based composite. Materials Science and Engineering: A, 157(1), 53-61.

40. Ye, H., and Liu, X. (2004). Review of recent studies in magnesium matrix composites. Journal of materials science, 39(20), 6153-6171.

41. Carreño-Morelli, E., Yang, J., Couteau, E., Hernadi, K., Seo, J. W., Bonjour, C., Forro,L. and Schaller, R. (2004). Carbon nanotube/magnesium composites. physica status solidi (a), 201(8), R53-R55.

42. Mizuuchi, K., Inoue, K., Hamada, K., Sugioka, M., Itami, M., Fukusumi, M., and Kawahara, M. (2004). Processing of TiNi SMA fiber reinforced AZ31 Mg alloy matrix composite by pulsed current hot pressing. Materials Science and Engineering: A, 367(1), 343-349.

43. Ye, H. Z., and Liu, X. Y. (2005). Microstructure and tensile properties of Ti6Al4V/AM60B magnesium matrix composite. Journal of alloys and compounds, 402(1), 162-169.

44. Xie, G., Ohashi, O., Yamaguchi, N., and Wang, A. (2003). Effect of surface oxide films on the properties of pulse electric-current sintered metal powders. Metallurgical and Materials Transactions A, 34(11), 2655-2661.

45. Munir, Z. A., Anselmi-Tamburini, U., and Ohyanagi, M. (2006). The effect of electric field and pressure on the synthesis and consolidation of materials: A review of the spark plasma sintering method. Journal of Materials Science, 41(3), 763-777.

46. Taylor, G. F. (1933). U.S. Patent No. 1,896,854. Washington, DC: U.S. Patent and Trademark Office.

47. Cremer, G. D. (1944). U.S. Patent No. 2,355,954. Washington, DC: U.S. Patent and Trademark Office.

48. Inque, K., and Saito, S. (1972). U.S. Patent No. 3,656,946. Washington, DC: U.S. Patent and Trademark Office.

49. Inoue, K. (1967). U.S. Patent No. 3,340,052. Washington, DC: U.S. Patent and Trademark Office.

50. Omori, M. (2000). Sintering, consolidation, reaction and crystal growth by the spark plasma system (SPS). Materials Science and Engineering: A, 287(2), 183-188.

51. Yu, L. G., Khor, K. A., and Sundararajan, G. (2002). Boriding of mild steel using the spark plasma sintering (SPS) technique. Surface and Coatings Technology, 157(2), 226-230.

52. Kopeliovich, D. (n.d.). Spark plasma sintering. Retrieved from http://www.substech.com/dokuwiki/doku.php?id=spark_plasma_sintering

53. Eriksson, M., Radwan, M., and Shen, Z. (2012). Spark plasma sintering of WC, cemented carbide and functional graded materials. International Journal of Refractory Metals and Hard Materials.

54. Stanciu, L. A., Kodash, V. Y., and Groza, J. R. (2001). Effects of heating rate on densification and grain growth during field-assisted sintering of α-Al2O3 and MoSi2 powders. Metallurgical and Materials Transactions A, 32(10), 2633-2638.

55. Zhou, Y., Hirao, K., Yamauchi, Y., and Kanzaki, S. (2003). Effects of heating rate and particle size on pulse electric current sintering of alumina. Scripta materialia, 48(12), 1631-1636.

56. Shen, Z., Johnsson, M., Zhao, Z., and Nygren, M. (2004). Spark plasma sintering of alumina. Journal of the American Ceramic Society, 85(8), 1921-1927.

57. Anselmi-Tamburini, U., Garay, J. E., Munir, Z. A., Tacca, A., Maglia, F., and Spinolo, G. (2004). Spark plasma sintering and characterization of bulk nanostructured fully stabilized zirconia: Part I. Densification studies. Journal of materials research, 19(11), 3255-3262.

58. Skandan, G., Hahn, H., Kear, B. H., Roddy, M., and Cannon, W. R. (1994). The effect of applied stress on densification of nanostructured zirconia during sinter-forging. Materials Letters, 20(5), 305-309.

59. Zhang, D., Fu, Z., Yuan, R., and Guo, J. (2004). Spark plasma sintering- A promising new technique and its mechanism. Multiphased Ceramic Materials: Processing and Potential, 65-75.

60. Nygren, M., and Shen, Z. (2003). On the preparation of bio-, nano-and structural ceramics and composites by spark plasma sintering. Solid State Sciences, 5(1), 125-131.

61. Wang, S. W., Chen, L. D., Hirai, T., and Kang, Y. S. (1999). Microstructure inhomogeneity in Al2O3 sintered bodies formed during the plasma-activated sintering process. Journal of materials science letters, 18(14), 1119-1121.

62. Xie, G., Ohashi, O., Chiba, K., Yamaguchi, N., Song, M., Furuya, K., and Noda, T. (2003). Frequency effect on pulse electric current sintering process of pure aluminum powder. Materials Science and Engineering: A, 359(1), 384-390.

63. Ozaki, K., Kobayashi, K., Nishio, T., Matsumoto, A., and Sugiyama, A. (2000). Sintering phenomena on initial stage in pulsed current sintering. Journal of the Japan Society of Powder and Powder Metallurgy, 47(3), 293-297.

64. Wong, E. W., Sheehan, P. E., and Lieber, C. M. (1997). Nanobeam mechanics: elasticity, strength, and toughness of nanorods and nanotubes. Science, 277(5334), 1971-1975.

65. Rao, C. N., Satishkumar, B. C., Govindaraj, A., and Nath, M. (2001). Nanotubes. ChemPhysChem, 2(2), 78-105.

66. Hassan, S. F., and Gupta, M. (2005). Enhancing physical and mechanical properties of Mg using nanosized Al 2 O 3 particulates as reinforcement. Metallurgical and Materials Transactions A, 36(8), 2253-2258.

67. Nguyen, Q. B., and Gupta, M. (2008). Increasing significantly the failure strain and work of fracture of solidification processed AZ31B using nano-Al_2O_3particulates. Journal of Alloys and Compounds, 459(1), 244-250.

68. Nguyen, Q. B., and Gupta, M. (2008). Enhancing compressive response of AZ31B magnesium alloy using alumina nanoparticulates. Composites Science and Technology, 68(10), 2185-2192.

69. Habibnejad-Korayem, M., Mahmudi, R., and Poole, W. J. (2009). Enhanced properties of Mg-based nano-composites reinforced with Al_2O_3 nano-particles. Materials Science and Engineering: A, 519(1), 198-203.

70. Jiang, Q. C., Li, X. L., and Wang, H. Y. (2003). Fabrication of TiC particulate reinforced magnesium matrix composites. Scripta Materialia, 48(6), 713-717.

71. Deng, K. K., Wu, K., Wu, Y. W., Nie, K. B., and Zheng, M. Y. (2010). Effect of submicron size SiC particulates on microstructure and mechanical properties of AZ91 magnesium matrix composites. Journal of Alloys and Compounds, 504(2), 542-547.

72. Saberi, Y., Zebarjad, S. M., and Akbari, G. H. (2009). On the role of nano-size SiC on lattice strain and grain size of Al/SiC nanocomposite. Journal of Alloys and Compounds, 484(1), 637-640.

73. Ferkel, H., and Mordike, B. L. (2001). Magnesium strengthened by SiC nanoparticles. Materials Science and Engineering: A, 298(1), 193-199.

74. Lan, J., Yang, Y., and Li, X. (2004). Microstructure and microhardness of SiC nanoparticles reinforced magnesium composites fabricated by ultrasonic method. Materials Science and Engineering: A, 386(1), 284-290.

75. Cao G, Konishi , H., Li, X. (2008) .Mechanical properties and microstructure of SiC-reinforced Mg-(2.4)Al-1Si nanocomposites fabricated by ultrasonic cavitation-based solidification processing. Materials Science and Engineering: A, 486(1), 357-362.

76. Wong, E. W., Sheehan, P. E., and Lieber, C. M. (1997). Nanobeam mechanics: elasticity, strength, and toughness of nanorods and nanotubes. Science, 277(5334), 1971-1975.

77. Rao, C. N., Satishkumar, B. C., Govindaraj, A., and Nath, M. (2001). Nanotubes. ChemPhysChem, 2(2), 78-105.

78. Morisada, Y., Fujii, H., Nagaoka, T., and Fukusumi, M. (2006). MWCNTs/AZ31 surface composites fabricated by friction stir processing. Materials Science and Engineering A, 419(1), 344-348.

79. Goh, C. S., Wei, J., Lee, L. C., and Gupta, M. (2006). Simultaneous enhancement in strength and ductility by reinforcing magnesium with carbon nanotubes. Materials Science and Engineering: A, 423(1), 153-156.

80. Goh, C. S., Wei, J., Lee, L. C., and Gupta, M. (2008). Ductility improvement and fatigue studies in Mg-CNT nanocomposites. Composites Science and Technology, 68(6), 1432-1439.

81. Li, Q., Viereckl, A., Rottmair, C. A., and Singer, R. F. (2009). Improved processing of carbon nanotube/magnesium alloy composites. Composites Science and Technology, 69(7), 1193-1199.

82. Kondoh, K., Fukuda, H., Umeda, J., Imai, H., Fugetsu, B., and Endo, M. (2010). Microstructural and mechanical analysis of carbon nanotube reinforced magnesium alloy powder composites. Materials Science and Engineering: A, 527(16), 4103-4108.

83. Geim, A. K., and Novoselov, K. S. (2007). The rise of graphene. Nature materials, 6(3), 183-191.

84. Singh, V., Joung, D., Zhai, L., Das, S., Khondaker, S. I., and Seal, S. (2011). Graphene based materials: Past, present and future. Progress in Materials Science, 56(8), 1178-1271.

85. Ramanathan, T., Abdala, A. A., Stankovich, S., Dikin, D. A., Herrera-Alonso, M., Piner, R. D., Adamson, D. H. , Schniepp , H. C. , Chen, X., Ruoff, R. S., Nguyen, S. T., Aksay, I. A., Prud'Homme, R. K. and Brinson, L. C. (2008). Functionalized graphene sheets for polymer nanocomposites. Nature nanotechnology, 3(6), 327-331.

86. Rafiee, M. A., Rafiee, J., Wang, Z., Song, H., Yu, Z. Z., and Koratkar, N. (2009). Enhanced mechanical properties of nanocomposites at low graphene content. Acs Nano, 3(12), 3884-3890.

87. Kuilla, T., Bhadra, S., Yao, D., Kim, N. H., Bose, S., and Lee, J. H. (2010). Recent advances in graphene based polymer composites. Progress in Polymer Science, 35(11), 1350-1375.

88. Kim, H., Abdala, A. A., and Macosko, C. W. (2010). Graphene/polymer nanocomposites. Macromolecules, 43(16), 6515-6530.

89. He, T., Li, J., Wang, L., Zhu, J., and Jiang, W. (2009). Preparation and Consolidation of Alumina/Graphene Composite Powders. Materials transactions, 50(04), 749-751.

90. Zhang, X.Y. , Li, H.P., Cui, X.L., Lin, Y. (2010). Graphene/TiO2 nanocomposites – synthesis characterization and application of hydrogen evolution from water photo-catalytic splitting. JMater Chem ,20, 2801–6.

91. Yang, S., Cui, G., Pang, S., Cao, Q., Kolb, U., Feng, X., Maier, J., and Müllen, K. (2010). Fabrication of Cobalt and Cobalt Oxide/Graphene Composites: Towards High-Performance Anode Materials for Lithium Ion Batteries. ChemSusChem, 3(2), 236-239.

92. Ding Y, Jiang Y, Xu F, Yin J, Ren H, Zhou Q .(2010). Preparation of nano-structured LiFePO4/graphene composites by coprecipitation method. Electrochem Commun, 12(1),10–3.

93. Wang, K., Wang, Y., Fan, Z., Yan, J., and Wei, T. (2011). Preparation of graphene nanosheet/alumina composites by spark plasma sintering. Materials Research Bulletin, 46(2), 315-318.

94. Fan, Y., Wang, L., Li, J., Sun, S., Chen, F. (2010). Preparation and electrical properties of graphene nanosheet/Al2O3 composites, Carbon, 48(1), 743–9.

95. Walker, L. S., Marotto, V. R., Rafiee, M. A., Koratkar, N., and Corral, E. L. (2011). Toughening in graphene ceramic composites. ACS nano, 5(4), 3182-3190.

96. Wang, J., Li, Z., Fan, G., Pan, H., Chen, Z., and Zhang, D. (2012). Reinforcement with graphene nanosheets in aluminum matrix composites. Scripta Materialia.

97. Chen, L. Y., Konishi, H., Fehrenbacher, A., Ma, C., Xu, J. Q., Choi, H.,Xu, H.F., Pfefferkorn, F.E., and Li, X. C. (2012). Novel Nanoprocessing Route for Bulk GrapheneNanoplatelets Reinforced Metal Matrix Nanocomposites. Scripta Materialia.

98. Muhammad, W. N. A. W., Sajuri, Z., Mutoh, Y., and Miyashita, Y. (2011). Microstructure and mechanical properties of magnesium composites prepared by spark plasma sintering technology. Journal of Alloys and Compounds, 509(20), 6021-6029.

99. Shen, J.F. , Hu, Y., Li, C., Qin, C., Shi, M. , Ye, M. (2009). Layer-by-Layer Self-Assembly of Graphene Platelets. Langmuir 25(11) 6122-6128

100. Barnett, M. R. (2007). Twinning and the ductility of magnesium alloys: Part II.“Contraction” twins. Materials Science and Engineering: A, 464(1), 8-16.

101. Umeda, J., Kondoh, K., Imai, H. (2009) .Friction and wear behavior of sintered magnesium composite reinforced with CNT-Mg2Si/MgO. Materials Science and Engineering A, 504(1), 157-162

102. Chua, B. W., Lu, L., and Lai, M. O. (1999). Influence of SiC particles on mechanical properties of Mg based composite. Composite Structures, 47(1), 595-601.

103. Szaraz, Z., Trojanova, Z., Cabbibo, M., and Evangelista, E. (2007). Strengthening in a WE54 magnesium alloy containing SiC particles. Materials Science and Engineering: A, 462(1), 225-229.

104. Dai, L. H., Ling, Z., and Bai, Y. L. (2001). Size-dependent inelastic behavior of particle-reinforced metal–matrix composites. Composites Science and Technology, 61(8), 1057-1063.

105. Clyne, T. W., and Withers, P. J. (1995). An introduction to metal matrix composites. Cambridge University Press.

106. Alpas, A.T., Zhang, J. (1992) .Effect of SiC particulate reinforcement on the dry sliding wear of aluminum-silicon alloys (A356). Wear, 155(1), 83–104

107. Alahelisten, A., Bergman, F., Olsson,M., Hogmark, S.(1993) On the wear of aluminum and magnesium metal matrix composites. Wear , 165 (1), 221–226

108. Abachi, P., Masoudi, A., and Purazrang, K. (2006). Dry sliding wear behavior of SiC_P / QE22 magnesium alloy matrix composites. Materials Science and Engineering: A, 435, 653-657.

VITA

Aniruddha Das

Candidate for the Degree of

Master of Science

Thesis: SPARK PLASMA SINTERING OF MAGNESIUM MATRIX COMPOSITES

Major Field: Mechanical and Aerospace Engineering

Biographical:

Education:

Completed the requirements for the Master of Science in Mechanical and Aerospace Engineering at Oklahoma State University, Stillwater, Oklahoma in December, 2012.

Completed the requirements for the Bachelor of Science in Mechanical Engineering at Bangladesh University of Science and Technology (BUET), Dhaka, Bangladesh in 2009.

Experience:

- 1 year and six months of experience of working as Graduate Research Assistant in Spark Plasma Sintering Lab in OSU.
- 1 year of experience of working as Graduate Teaching Assistant in Machine Design Lab at OSU.
- Authored 1 conference paper in International Conference in Mechanical Engineering, Dhaka, Bangladesh

Name: Aniruddha Das Date of Degree: December, 2012

Institution: Oklahoma State University Location: Stillwater, Oklahoma

Title of Study: SPARK PLASMA SINTERING OF MAGNESIUM MATRIX COMPOSITES

Pages in Study: 77 Candidate for the Degree of Master of Science

Major Field: Mechanical and Aerospace Engineering

Magnesium (Mg) is widely used as a structural material due to its low density (1.74 g/cm^3), high specific strength and good machinability. Due to these intrinsic properties, magnesium is being used in aerospace and automobile industries as a replacement of steel and aluminum. Moreover, it is also used as a replacement of plastics in electronics and computer industries. However, Mg shows poor wear resistance. In this thesis, efforts are directed towards synthesizing high strength magnesium matrix composites having excellent wear resistance.

In this work, graphene platelets (GPL) and nano SiC reinforced Mg matrix composites were synthesized using spark plasma sintering (SPS) technique. SPS is a novel nanoprocessing method where uniaxial pressure and pulse direct current are applied simultaneously to consolidate powders. Mg-GPL matrix composites exhibited improved hardness and ductility. In Mg-nano SiC composites, significant improvement of hardness and ultimate compressive strength was observed. GPL and nano-SiC particles also resulted in substantial improvement in tribological properties due to the lubrication effect of GPL and the defensive mechanism by hard nano-SiC particles.

ADVISER'S APPROVAL: Sandip P. Harimkar